Innate Antifungal Immune Receptor, Dectin-1, Undergoes Ligand-Induced Oligomerization with Highly Structured β-Glucans and at Fungal Cell Contact Sites

Authors:

Eduardo U. Anaya[1], Akram Etemadi Amin[1,2], Mike Danielson[3], Kyle Michel[3], Aaron K. Neumann[1,4]

Affiliations:

1. Department of Pathology, University of New Mexico, School of Medicine, Albuquerque, NM, USA, 87131

2. Department of Physics and Astronomy, University of New Mexico, Albuquerque, NM, USA 87131

3. ImmunoResearch Inc., Eagan, MN, USA, 55121

4. Corresponding author: akneumann@salud.unm.edu

Keywords:

Dectin-1, dimer, beta-glucan, *Candida albicans*, hemITAM, Syk, Calcium signaling, FRET, RICS, N&B

Author Summary

Candidemia is the most common bloodstream infection in the United States. During infection, the fungal cell wall is an important virulence factor, playing roles in adhesion, immune recognition and colonization. The human innate immune system recognizes β-glucan, a highly immunogenic component of the fungal cell wall. During innate immune recognition of *Candida*, the organization of cell wall β-glucan is an important determinant of a successful immune activation. However, there have been many reports showing conflicting biological activities of β-glucans with different size, branching and structure. Here, using quantitative fluorescence imaging techniques, we investigate how differential size and structure of β-glucan impacts activation of the innate immune receptor, Dectin-1A. Our results indicate a positive correlation between highly structured glucans and Dectin-1A activation. Furthermore, we determined this is due to the higher ordered β-glucan causing Dectin-1A receptors to form aggregates that are below 15 nm in size. Finally, Dectin-1A receptor aggregation has also been shown to form at fungal particle contact sites with high β-glucan exposure.

Abstract

Dectin-1A is a C-type Lectin innate immunoreceptor that recognizes β-(1,3:1,6)-glucan, a structural component of *Candida* species cell walls. The higher order structure of β-glucans ranges from random coil to insoluble fiber due to varying degrees of tertiary (helical) and quaternary structure. Model *Saccharomyces cerevisiae* β-glucans of medium and high molecular weight (MMW and HMW, respectively) are highly structured. In contrast, low MW glucan (LMW) is much less structured. Despite similar affinity for Dectin-1A, the ability of glucans to induce Dectin-1A mediated calcium influx

and Syk phosphorylation positively correlates with their degree of higher order structure. Chemical denaturation and renaturation of MMW glucan showed that glucan structure determines agonistic potential, but not binding affinity, for Dectin-1A. We explored the role of glucan structure on Dectin-1A oligomerization, which is thought to be required for Dectin-1 signaling. Glucan signaling decreased Dectin-1A diffusion coefficient in inverse proportion to glucan structural content, which was consistent with Dectin-1A aggregation. Förster Resonance Energy Transfer (FRET) measurements revealed that molecular aggregation of Dectin-1 occurs in a manner dependent upon glucan higher order structure. Number and Brightness analysis specifically confirmed an increase in the Dectin-1A dimer and oligomer populations that is correlated with glucan structure content. Receptor modeling data confirms that in resting cells, Dectin-1A is predominantly in a monomeric state. Super Resolution Microscopy revealed that glucan-stimulated Dectin-1 aggregates are very small (<15 nm) collections of engaged receptors. Finally, FRET measurements confirmed increased molecular aggregation of Dectin-1A at fungal particle contact sites in a manner that positively correlated with the degree of exposed glucan on the particle surface. These results indicate that Dectin-1A senses the solution conformation of β-glucans through their varying ability to drive receptor dimer/oligomer formation and activation of membrane proximal signaling events.

Introduction

Overall, *Candida* infections have increased over the past 20 years in the United States [1–5]. It is estimated that 46,000 cases of healthcare-associated invasive candidiasis

occur in the United States annually [6]. The fungal cell wall is composed of an inner layer of chitin, a middle layer of β(1,3:1,6)-D-glucan and an outer layer of N- and O-linked mannans [7]. During infection, the cell wall of *Candida* is an important and relevant virulence factor, playing roles in adhesion, colonization and immune recognition [8,9]. Due to the abundant amount of mannan on the cell wall, β-glucan exhibits a very limited, punctate pattern of nanoscale surface exposure. The extent of this glucan masking is influenced by environmental conditions such as intestinal pH or lactate levels [10,11]. In addition, interactions with neutrophils have been shown to “unmask” the mannose layer through a neutrophil extracellular trap-mediated mechanism [12]. Furthermore, our lab and others have determined that anti-fungal drugs “unmask” the fungal cell wall, which leads to increases in nanoscale regions of glucan exposure and correlates with enhanced host defense [13–15]. Therefore, fungal species use masking as a way to evade recognition of β-glucan by the host’s immune system [16].

β-glucans consist of a β-1,3-linked backbone with side chains of β-1,6-linked units that vary in length and degree of branching [17]. β-glucan forms triple-helical structures through intermolecular hydrogen bonds with two other strands [17–21]. This triple helix conformation has been shown to form with just the β-1,3-linked backbone, however β-1,6-linked side chains play an important role in determination of the triple helix cavity formation through side chain/side chain interactions [21].

β-glucans are known for their biological activities such as enhancing anti-tumor, anti-bacterial, and anti-viral immunity as well as in wound healing [22–25]. The biological activity of glucan is affected by its structure, size, chemical modification, conformation and solubility [26]. Research has found that branching is not required to observe

biological activity, but branching has been shown to enhance binding to the Dectin-1 receptor [27]. In contrast, β-glucan size is thought to play a major role in biological activity with glucans that are shorter than 10,000 Da often being biologically inactive [28,29]. However, despite having similar sizes, glucans can display differences in their biological activities [30–32]. For example, studies have demonstrated that the immunoregulatory activity of laminarin varies between agonistic and antagonistic depending on its physicochemical properties, purity and structure [33]. Furthermore, β-glucans that have a triple helical conformation are more potent agonists of host immune response than single helical glucan [34–37]. We propose that the β-glucan triple-helix conformation plays an important role in determining the biological activity of the β-glucan through modulating the degree of receptor oligomerization upon ligation.

During innate immune recognition of *Candida*, the organization of cell wall ligands and pattern recognition receptors is an important determinant of successful immune activation [8]. The C-type lectin (CTL) anti-fungal immunoreceptors play a central role in the detection of *Candida* during bloodstream infection [38]. Dectin-1A is the main CTL that recognizes the soluble and particulate β-glucan found in the fungal cell wall [39–41]. Dectin-1A is found in myeloid lineage cells, and once activated, it stimulates phagocytic activity, the production of reactive oxygen intermediates and inflammatory mediators. Dectin-1A contains a CTL-like domain, separated from the cell membrane by a glycosylated stalk region, a transmembrane domain and an intracellular cytosolic domain. The cytosolic tail contains half an Immunoreceptor Tyrosine-based Activation Motif (a YXXL sequence with an upstream stretch of acidic amino acids) in its cytoplasmic tail and so is termed a (hem)ITAM receptor [42,43]. Monophosphorylated

113 ITAM domains poorly recruit and activate Syk for downstream signaling [44], suggesting
114 that hemITAM domains with their single phosphotyrosine site would be poorly activating
115 in a monomeric configuration. Consistent with this hypothesis, another (hem)ITAM
116 bearing receptor, CLEC-2, is reported to require dimerization for its signaling [45]. By
117 analogy to this and other (hem)ITAM receptors, it is hypothesized that Dectin-1A must
118 oligomerize to recapitulate a multivalent binding site for Syk and to facilitate signal
119 transduction [8,45,46]. However, this prediction has not been directly explored for
120 Dectin-1A in live cells at the molecular level with relation to structural determinants of
121 receptor-ligand complex organization and signaling outcomes.

122 In this study, we propose that factors that induce an aggregated membrane organization
123 of Dectin-1A during activation are very important for determining signaling outcomes of
124 Dectin-1A engagement by β-glucan [45,46]. We hypothesize that ligand structure
125 impacts signaling by determining the membrane organization and spatiotemporal
126 clustering dynamics of Dectin-1A. To test this hypothesis, we stimulated HEK-293 cells
127 transfected with Dectin-1A with a variety of soluble β-glucans that have different
128 structures and sizes. We chose to work in this model system because it provides a
129 simplified platform necessary to investigate the physical biology of Dectin-1A activation
130 by isolating Dectin-1A signaling from the complex milieu of other receptors and other
131 Dectin-1 isoforms expressed in innate immunocytes. Also, this model facilitates the
132 expression of multiple fluorescent protein-tagged Dectin-1A constructs necessary to the
133 work. Using calcium imaging and western blotting assays, our results revealed that
134 Dectin-1A activation is influenced by the β-glucan triple helical structure. Furthermore,
135 our subcellular FRET measurements by Fluorescence Lifetime Imaging Microscopy

136 (FLIM-FRET), as well as application of fluorescence correlation spectroscopy
137 approaches, revealed dimerization and oligomerization of Dectin-1A when stimulated
138 with highly structured β-glucans. In addition, these dimerization events occurred in
139 fungal contact sites of fungal cells with high glucan exposure. Together, our findings
140 indicate β-glucan structure is required for Dectin-1A to form signaling-competent dimeric
141 and oligomeric membrane aggregates.

142

143 **Results:**

144 **Dectin-1A activation is dependent on the molecular weight of the soluble β-**
145 **glucan.**

146 β-glucans, existing as insoluble fibers in the cell wall, are likely to have a high degree of
147 tertiary and quaternary structure. So, an encounter with highly structured glucan might
148 be indicative of a pathogen cell wall structure. Furthermore, less structured glucans are
149 encountered by Dectin-1A physiologically [42]. Small soluble circulating glucan can
150 derive from sloughed cell wall material or from dietary absorption [47–50]. However,
151 there is not much known about Dectin-1A's ability to distinguish between highly
152 structured β-glucan found on cell walls of fungal pathogens and less structured glucans
153 found in circulation. Therefore, we examined how Dectin-1A activation is affected by
154 glucans with different quaternary and tertiary structures. To accomplish this, we used
155 high molecular weight (HMW 450 kDa), medium molecular weight (MMW 145 kDa), and
156 low molecular weight (LMW 11 kDa) soluble glucans, in decreasing order of tertiary and
157 quaternary structures, derived from *S. cerevisiae* cell walls. These *S. cerevisiae* glucans

158 in soluble form or as particulate “zymosan” are common models for stimulation of innate
159 immunocytes by fungal pathogen cell wall glucan. The above glucans have overall very
160 similar composition and structures to *C. albicans* yeast glucan, though relatively minor
161 differences in β-(1,6)-glucan side chain length and branching frequency have been
162 reported between these species [51,52].

163 Using these glucans, we performed intracellular calcium ($[Ca^{2+}]_i$) measurement
164 experiments using HEK-293 cells transfected with Dectin-1A. We stimulated the cells
165 using either LMW, MMW, or HMW (Fig.1A). We found that large, highly ordered glucans
166 (HMW and MMW) induced more than a two-fold increase in peak amplitude of $[Ca^{2+}]_i$. In
167 contrast, the glucans with a random coil structure (LMW) showed little induction of
168 calcium signaling compared to unstimulated cells. These results indicate that Dectin-1A
169 drives differential Ca^{2+} flux to glucan ligands that vary in size and structure.

170 To determine how these differently structured soluble glucans impacted cellular patterns
171 of Syk phosphorylation, we stimulated HEK-293 cells expressing Dectin1A-mEmerald
172 with H_2O (vehicle), LMW, MMW, or HMW. Whole cell lysate was collected and Syk
173 phosphorylation was determined by western blot analysis. Likewise, our results show an
174 increase in Syk phosphorylation in the larger, highly structured glucan MMW and HMW
175 compared to unstimulated and LMW stimulated cells (Fig. 1B). Additionally, Syk
176 inhibitors abrogated calcium signaling of Dectin-1A when stimulated with MMW glucan
177 (Fig. 1C). These results indicate that glucans with higher order structure are better able
178 to activate Dectin-1A-mediated Ca^{2+} signaling and that this is a Syk dependent process.

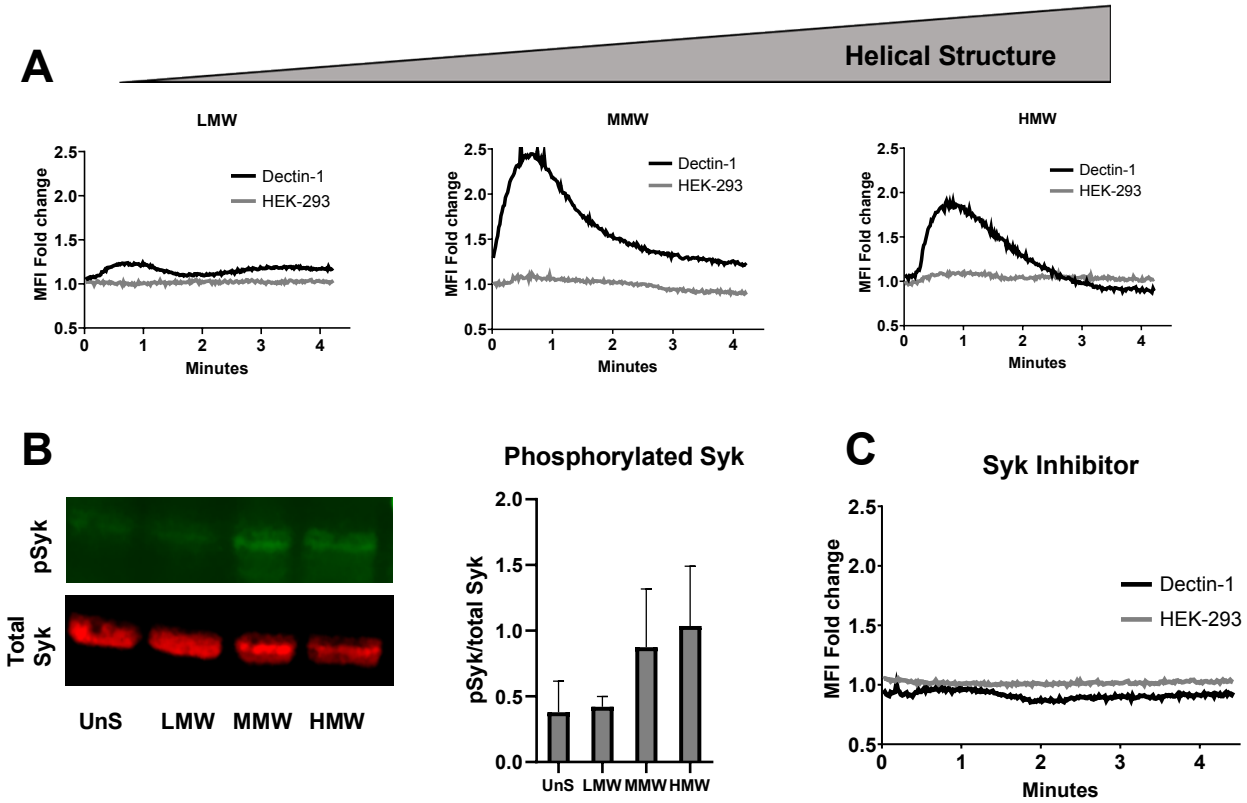

179

180 **Figure 1. Differential signaling response to soluble β-glucan for Dectin-1A.**

181 (A) HEK-293 cells stably transfected with Dectin-1A were loaded with Fluo-4 and Cell Tracker Deep Red
182 at equimolar concentrations. Cell Tracker Deep Red was simultaneously loaded in order to normalize for
183 changes in cytosolic volume caused from cell movement during observation. Mean fluorescence intensity
184 was observed for Dectin-1A transfected (black) or untransfected (grey) HEK-293 cells stimulated with
185 LMW, MMW, or HMW at 1 ug/ml. (n = 30 per glucan from 3 independent experiments per glucan). Data
186 shown as mean fold change in volume-normalized $[Ca^{2+}]_{intracelullar}$. (B) Cell lysates were collected at 5 min
187 after stimulation and analyzed by Western blotting using antibodies against p-Syk and Syk. The intensity
188 of p-Syk was normalized against total Syk. Representative western blot on the left. Quantification of the
189 western blot data (right) shown as mean ± SD are relative intensity of p-Syk (n = 3). (C) Untransfected
190 (grey) and stably transfected Dectin-1A (black) HEK-293 cells were loaded with Fluo-4 and Cell Tracker
191 Deep Red at equimolar concentrations and treated with Syk Inhibitor at 250 nM and stimulated with

192 MMW. Mean fluorescence intensity was observed for cells stimulated with MMW at 1 ug/ml. (n = 30 from
193 3 independent experiments).

194

195 **β-glucan denaturation does not induce Dectin-1A activation**

196 To specifically determine if the glucan structure affects signaling outcomes, we
197 denatured MMW (highly stimulatory glucan) using DMSO, which inhibits the formation of
198 tertiary structures, thus converting MMW's triple helix structure to a single helical
199 structure [17]. The results showed that when we denatured these glucans, we did not
200 observe calcium signaling in cells expressing Dectin-1A (Fig. 2A). However, when we
201 renatured the glucans by removing DMSO via dialysis we observe partial recovery of
202 calcium signaling. In addition, we confirmed the loss of helical structure via a Congo
203 Red assay. Congo Red specifically binds to β-1,3-D-glucans with a triple helix
204 conformation as their tertiary structure. This binding is detected by bathochromic shift in
205 absorbance maximum from 488 to 516 nm [53]. Our results indicated a loss in glucan
206 structure after denaturation in a DMSO solution that was regained upon renaturation
207 (Fig. 2B). Moreover, we repeated these experiments by stimulating cells with glucan
208 denatured with NaOH or neutralized renatured glucan [17]. Similarly, our results show
209 that denatured MMW does not stimulate Dectin-1A signaling, but agonistic potential of
210 this glucan is partially regained when the glucan is renatured (Fig. 2C). In addition, we
211 confirmed that glucan structure was lost when NaOH was added and regained when
212 neutralized with HCl (Fig. 2D). These results suggest that glucan structure is an
213 important factor in activating a Dectin-1A response.

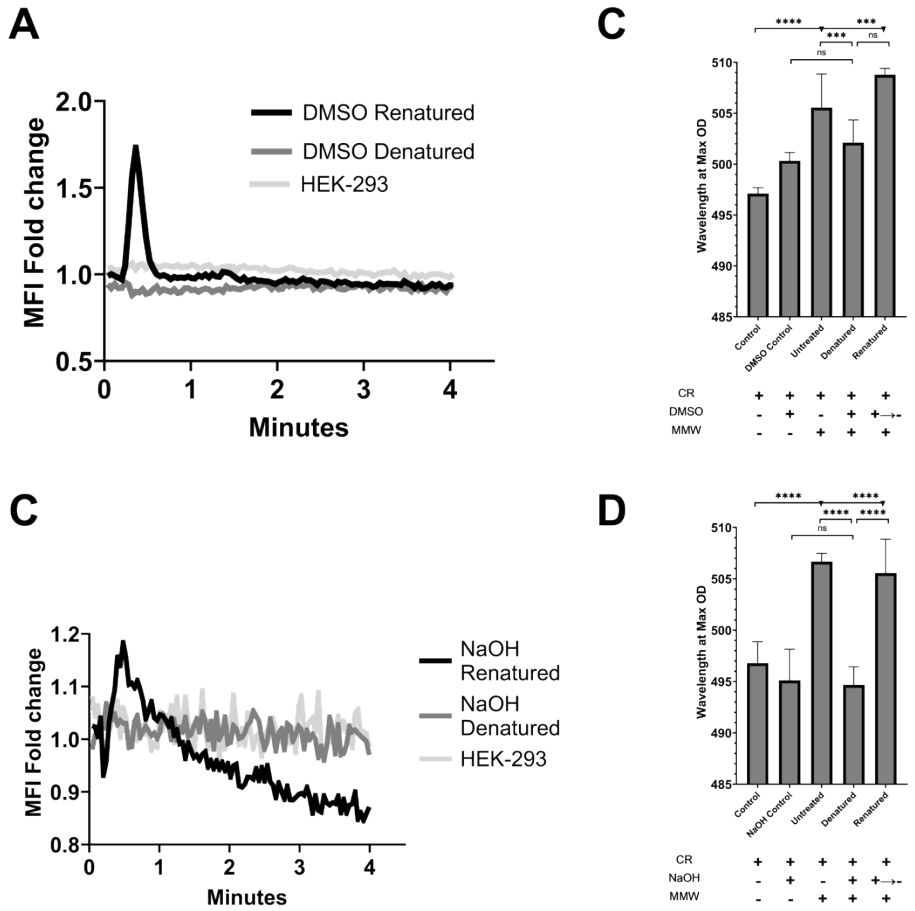

Figure 2: Denaturation of highly structured glucan causes it to lose its stimulatory potential.

(A) HEK-293 cells stably expressing Dectin-1A or untransfected were loaded with Fluo-4 and Cell Tracker Deep Red at equimolar concentrations. Mean fluorescence intensity was observed for cells stimulated with DMSO denatured/renatured MMW. (n = 30 from 3 independent experiments). (B) 1 mg/ml of MMW glucan was denatured using DMSO and incubated with 8μM Congo Red. Control samples contained Congo Red with and without DMSO to illustrate the extent of red shift attributable to solvent effects alone. Renaturation was accomplished by dialyzing out DMSO 24 hrs prior to the experiment. Data shown as mean ± SD (n = 9 from 3 independent experiments). (C) HEK-293 cells stably expressing Dectin-1A or untransfected were loaded with Fluo-4 and Cell Tracker Deep Red at equimolar concentrations. Mean fluorescence intensity was observed for cells stimulated with NaOH denatured/renatured MMW at 1

226 ug/ml. (n = 30 from 3 independent experiments). Data shown as mean. (D) 1 mg/ml of MMW glucan was
227 denatured using NaOH and incubated with 8 μM Congo Red. Control samples contained Congo Red with
228 and without Congo Red to assess denaturant effect on the optical properties of the dye, but the presence
229 of denaturant had no significant effect on Congo Red in this case. Renaturation was accomplished by
230 neutralizing NaOH 24 hrs prior to the experiment. Data shown as mean ± SD (n = 9 from 3 independent
231 experiments). Welch's t-test, ** $p<0.001$, *** $p<0.0001$, **** $p<0.000001$.

232 **β-glucan structure and affinity**

233 We considered the possibility that these soluble glucans might have different affinities
234 for Dectin-1A, resulting in differential receptor activation. Thus, we conducted Biolayer
235 Interferometry experiments to determine the binding affinity of these glucans to the
236 carbohydrate recognition domain of Dectin-1A. This was accomplished using a chimeric
237 fusion protein of the carbohydrate recognition domain of Dectin-1A and the human IgG
238 Fc region. An anti-human IgG Fc Capture biosensor tip was used to load this fusion
239 protein. Association and dissociation curves of the soluble glucan were then collected.
240 The results shown in Fig. 3A indicate that all the glucans have approximately nanomolar
241 dissociation constants for Dectin-1A carbohydrate recognition domain despite the
242 previously described differences in signaling [27]. Weight average molecular weights of
243 purified *Saccharomyces cerevisiae* β -(1,3)-glucan fractions vary over an approximate
244 40-fold range, but there is relatively little difference between these glucans' apparent
245 affinity for the Dectin-1A carbohydrate recognition domain.

246 Furthermore, to quantify differences in the helical structure possessed by LMW, MMW
247 and HMW glucans, we analyzed the conformational transition of triple helix to random
248 coil of β-1,3-D-glucans through denaturation experiments. Experiments were conducted
249 by denaturing glucans with NaOH at various concentrations in the presence of Congo

250 Red. Our results show that the amount of glucan tertiary structure scales with molecular
251 weight as measured by the concentration of NaOH required to reduce Congo Red
252 binding to glucan to half-maximal values (Fig. 3B), suggesting that the size of the
253 glucans is correlated with their structure. This result was expected because larger
254 glucans are able to engage in more extensively in interstrand hydrogen bonding
255 interactions that maintain triple helical structures. Together, these results indicate that
256 downstream signaling of the receptor is determined by the structure of the glucan rather
257 than affinity alone.

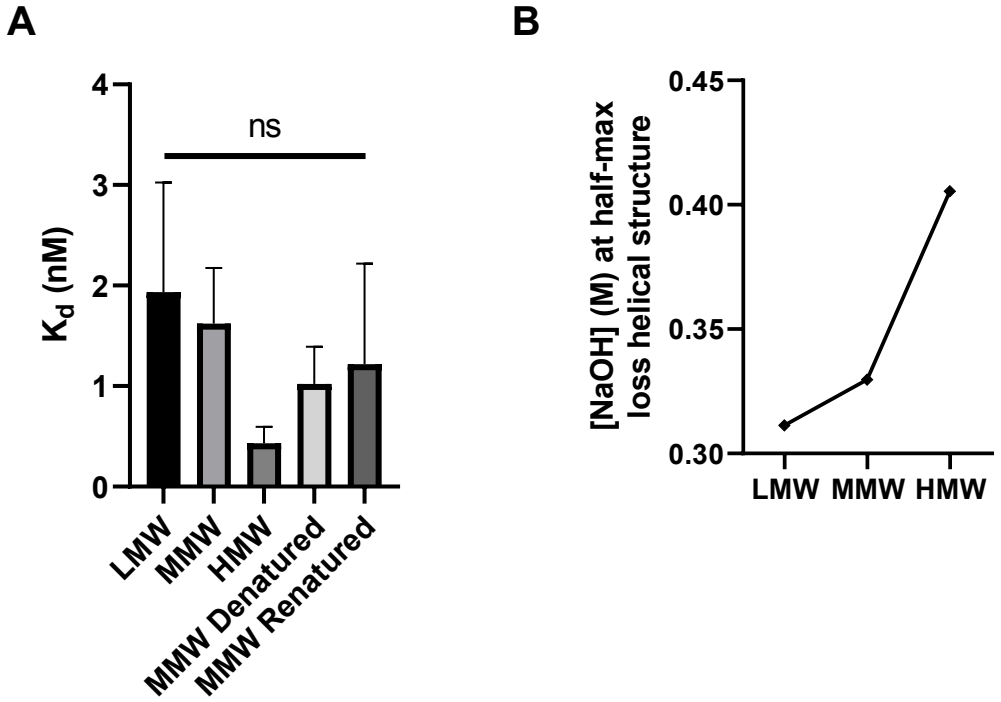

258

259 **Figure 3: Characterization of fungal cell wall glucans used in this study.**
260 **Characterization of untreated, denatured and renatured β-glucans.**

261 (A) Biolayer Interferometry experiments were conducted on LMW, MMW, HMW, MMW denatured, and
262 MMW renatured glucans using an anti-human IgG Fc Capture biosensors tip and a Dectin-1A-Fc fusion
263 protein. Data shown as mean ± SD (n = 3 from 3 independent experiments). (B) LMW, MMW, and HMW

264 β-glucans were denatured using 0M-1M of NaOH in the presence of 8.8 μM Congo Red. Concentration of
265 NaOH at which absorbance decreased to the half-maximal value were plotted. Data shown as mean ± SD
266 (n = 9 from 3 independent experiments); One-way ANOVA test was conducted.

267

268 Dectin-1A decreases in diffusion and receptor density when stimulated with 269 highly structured β-glucans

270 The Stokes-Einstein equation predicts that if a diffusing object increases in
271 hydrodynamic radius, it will slow down proportionally to that change. We measured the
272 diffusion coefficient of Dectin-1A pre/post glucan stimulation to determine whether
273 receptor diffusion coefficient decreased, potentially due to increasing hydrodynamic
274 radius as an initially monomeric receptor formed larger clusters/oligomers. We obtained
275 average diffusion coefficients and spatial number density of our receptor using Raster
276 Image Correlation Spectroscopy (RICS). Previous research has described RICS in
277 more detail [54,55]. Briefly, we generated a volume of excitation using a confocal laser
278 and calibrated this volume using standard fluorophores of known diffusion coefficient.
279 We then observed fluorescent molecules (i.e., Dectin-1A-mEmerald) diffusing in and out
280 of this excitation volume through fluctuation in the number of photons obtained.
281 Experimentally observed florescence correlations at various spatiotemporal lags were
282 then fit to a 2D autocorrelation function to obtain receptor diffusion coefficient and
283 spatial density in the observed membrane.

284 Using HEK-293 cells expressing Dectin-1A-mEmerald, we conducted RICS
285 measurements before and after stimulation with soluble β-glucans. We determined that
286 cells stimulated with MMW or HMW exhibited a significant decrease in mobility

287 compared to LMW and unstimulated cells (Fig. 4A). This finding is consistent with an
288 increase in receptor aggregation upon stimulation, which we examine in greater detail
289 below. Moreover, we observed a significant decrease in receptor density after treatment
290 with MMW or HMW, compared to non-simulated or LMW cells (Fig. 4B). This finding
291 might be explained by receptor internalization after stimulation by MMW or HMW. While
292 RICS analysis does use detrending to remove immobile and very low mobility receptor
293 from analysis, we do note that progressive confinement of activated receptors in
294 nascent endocytic structures could also potentially contribute to the decreased apparent
295 diffusion coefficient we observed post-stimulation. So, we proceeded to conduct more
296 detailed membrane biophysical studies to specifically assess the molecular aggregation
297 state of Dectin-1 during stimulation with glucan.

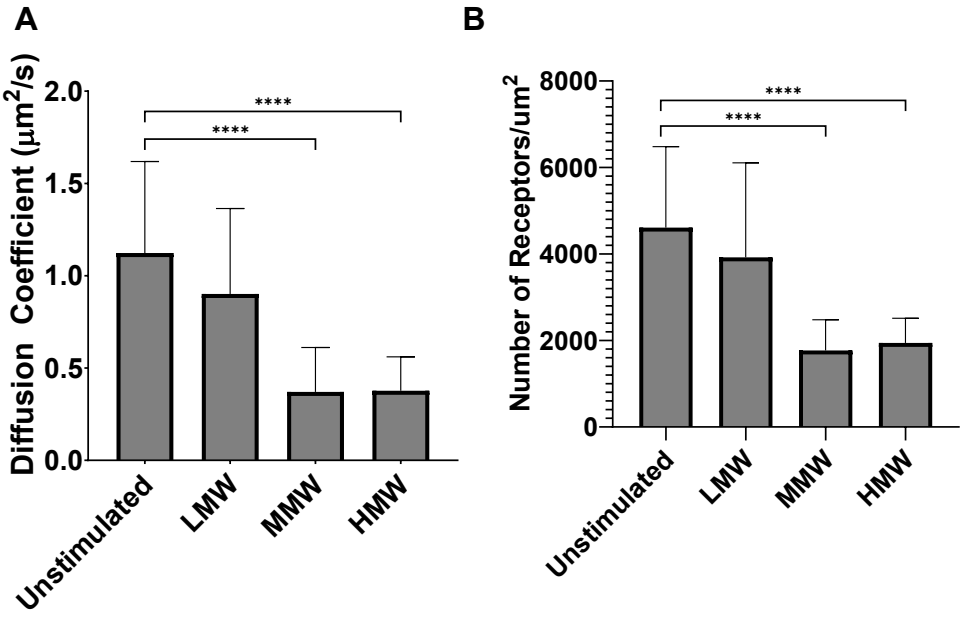

298

299 **Figure 4: Dectin-1A surface diffusion and receptor numbers decrease when**
300 **stimulated with highly structured β-glucans.**

301 (A). Raster Image Correlation Spectroscopy (RICS) analysis of fluorescently tagged Dectin-1A expressed
302 in HEK-293 provided average diffusion coefficient and (B) average receptor number for cells that were
303 unstimulated or stimulated with LMW, MMW, or HMW. Data shown as mean ± SD (n = 30); One-Way
304 ANOVA multiple comparison test, **** $p<0.00001$.

305

306 Dectin-1A forms dimers/oligomers when stimulated with highly structured β-
307 glucans

308 The results shown above indicate that the β-glucan structure is an important factor in
309 signaling outcomes. Previous research has shown that other transmembrane CTLs that
310 also contain a (hem)ITAM domain can form homodimers before or upon ligand
311 recognition [56,57]. Furthermore, crystallography studies of the carbohydrate
312 recognition domain (CRD) have shown that Dectin-1A head groups form dimers when
313 laminarin is present [58]. Additionally, size exclusion chromatography with multi-angled
314 light scattering analysis has described Dectin-1 ligand-induced tetramer formation in
315 solution [59]. In line with these ideas, we sought to examine how ligand structure
316 impacts signaling by determining the dimerization/oligomerization of full length Dectin-
317 1A in living cell membranes.

318 To accomplish this, we first employed Fluorescence-Lifetime Imaging Microscopy for
319 Forster Resonance Energy Transfer (FLIM-FRET). FRET based imaging capitalizes on
320 close proximity of two proteins to visualize protein-protein interactions, including
321 receptor dimerization and receptor-ligand complex formation [60]. FLIM characterizes
322 the duration of a fluorophore's excited state before returning to the ground state. The
323 occurrence of FRET causes rapid quenching of donor fluorescence, so FRET can be

324 determined by measuring the shortening of donor fluorescence lifetime when in
325 proximity to acceptor. FLIM-FRET offers the opportunity of studying *in vivo* receptor
326 interactions in a direct, spatially resolved manner. We examined Dectin-1A engagement
327 using FLIM-FRET on HEK-293 cells co-expressing fluorescent proteins Dectin-1A-
328 mEmerald (donor) and -mCherry (acceptor). The proteins used for experimental
329 determination of ligation-dependent Dectin-1A aggregation possessed fluorescent
330 proteins on the protein N-terminus (cytoplasmic tail), while a negative control for FRET
331 utilized donor and acceptor-tagged proteins on opposite sides of the membrane.
332 Analysis was conducted on the plasma membrane itself by masking out internal cellular
333 compartments (Fig. 5A). In the experiments, FRET efficiency is a parameter that
334 exhibits an inverse 6th power dependence upon donor-acceptor distance. Donor-
335 acceptor percentage is simply the percentage of all donors that are involved in FRET
336 interactions at a given time. These parameters are determined experimentally by
337 performing bi-exponential curve fits to the observed frequency distribution of donor
338 fluorophore lifetimes, wherein one exponential component represents the population of
339 non-FRET monomeric donors and the other exponential component represents the
340 performance of the donors that are involved in FRET interactions.

341 First, we characterized the average lifetimes of unstimulated cells expressing several
342 configurations of fluorescent protein tagged Dectin-1A: 1) receptor with donor tag only,
343 2) co-expression of separate donor and -acceptor tagged receptors with tags placed on
344 opposite sides of the plasma membrane (a negative control containing both fluorescent
345 proteins but in a configuration that does not permit FRET), and 3) co-expression of
346 separate donor and acceptor-tagged receptors with both tags in the cytoplasmic tail of

347 the receptors (configuration to be used for experimental determination of receptor
348 aggregation by FRET). The observed decay curves were analyzed by performing a bi-
349 exponential fit. For donor only (1) and our negative control (2), we observed a negative
350 amplitude for one of the bi-exponential lifetime fit components, indicating that a mono-
351 exponential fit was a more appropriate method of analysis. Our results showed that
352 when acceptor was not present, we see an average of 2.4 ns lifetime (Fig. 5B).
353 Negative controls with donor and acceptor on opposite sides of the membrane yielded
354 similar lifetime values. FLIM data from cells with co-expression of donor or acceptor-
355 tagged (cytoplasmic tail) Dectin-1A was fit bi-exponentially with the first component
356 fixed to the donor only lifetime (2.4 ns) and the lifetime of the second component was
357 reported. In this case, resting cells exhibited a decrease in the lifetime of the donor to
358 0.41 ns indicating that some basal level of intermolecular Dectin-1 close proximity
359 interactions were being observed in unstimulated cells. The existence of this basal
360 FRET signal is interesting, and the potential sources and interpretation of this
361 observation are considered in a section below. However, we first focused on assessing
362 ligation-dependent changes in Dectin-1A's molecular aggregation state as influenced by
363 various glucans and measured by FRET.

364 When we stimulated cells expressing Dectin-1A with donor and acceptor on the
365 cytoplasmic face of the membrane using MMW (Fig. 5D) or HMW (Fig. 5E), we saw a
366 significant increase in the number of receptors undergoing FRET (Donor-Acceptor
367 population) from 15% before stimulation to a maximum of 30% after 5 minutes of
368 stimulation, with observations starting at one minute post-stimulation. However, there
369 was not a significant change in FRET efficiency before and after stimulation. On the

370 other hand, when we stimulate with LMW (Fig. 5C) or denatured MMW (Fig. 5F), we
371 see no significant change in FRET efficiency or donor-acceptor population. We interpret
372 the high and constant FRET efficiency for the population of receptors engaged in FRET
373 interactions to mean that Dectin-1A in its aggregated state is in a close, well-defined
374 configuration that does not permit a wide range of separations between donor and
375 acceptor tags, leading to a constant FRET efficiency for the donor population that does
376 attain this FRET-capable configuration. However, the size of the population of receptors
377 engaged in these close molecular aggregates does change as a result of stimulation
378 with glucan. These results suggest that the highly structured soluble glucans allow for
379 an increase in Dectin-1A dimerization or oligomerization to occur, which directly
380 correlates with the amount of receptor activation and signaling observed.

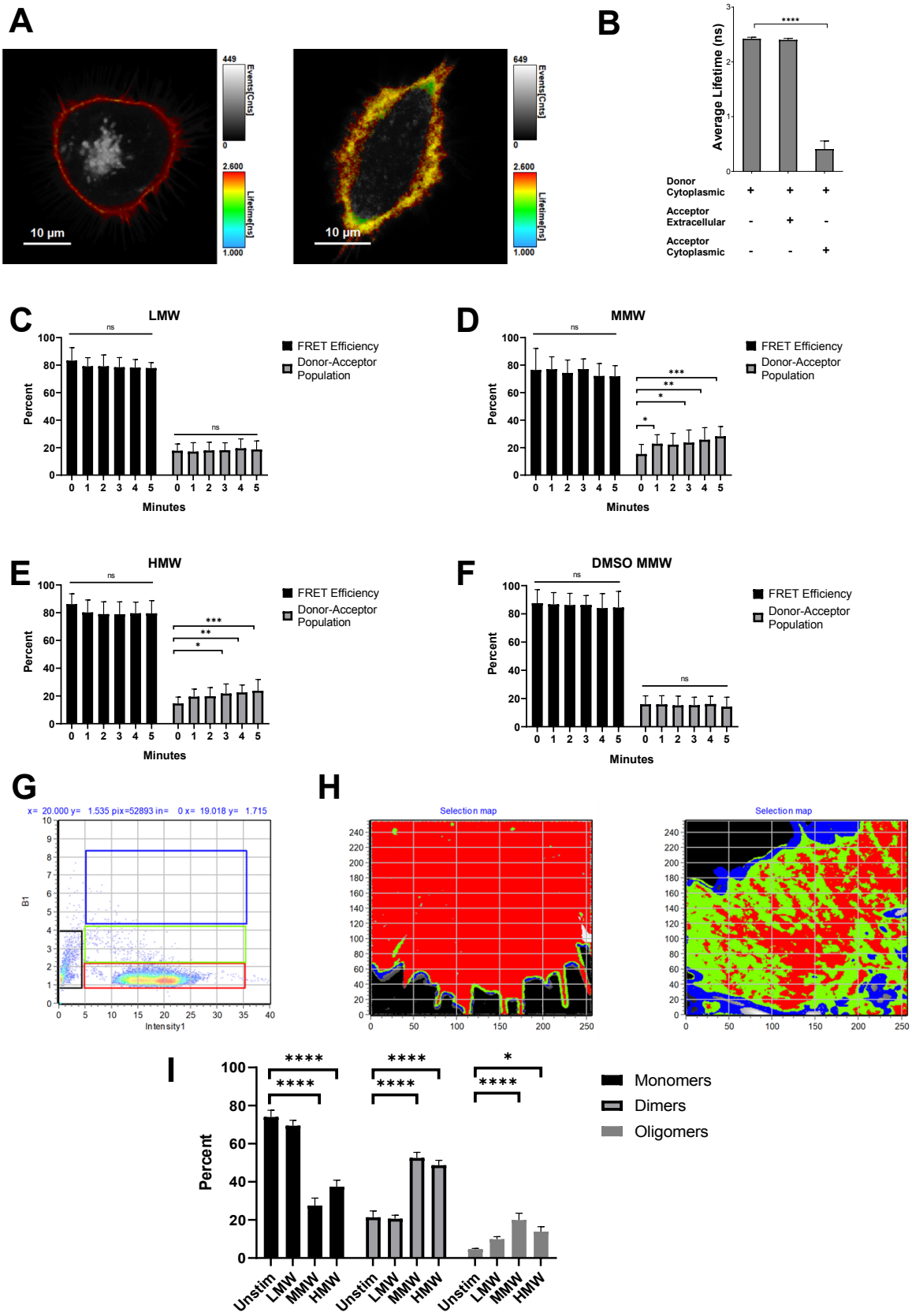
A
449
Events[Cnts]
0
2.600
Lifetime[ns]
1.000
10 µm
649
Events[Cnts]
0
2.600
Lifetime[ns]
1.000
10 µm
B
Average Lifetime (ns)
****
Donor Cytoplasmic + + +
Acceptor Extracellular - + -
Acceptor Cytoplasmic - - +
C
LMW
Percent
Minutes
ns
FRET Efficiency
Donor-Acceptor Population
D
MMW
Percent
Minutes
ns
***
**
*
FRET Efficiency
Donor-Acceptor Population
E
HMW
Percent
Minutes
ns
***
**
*
FRET Efficiency
Donor-Acceptor Population
F
DMSO MMW
Percent
Minutes
ns
FRET Efficiency
Donor-Acceptor Population
G
x= 20.000 y= 1.535 pix=52893 in= 0 x= 19.018 y= 1.715
B1
Intensity1
H
Selection map
Selection map
I
Percent
****
****
****
****
*
****
Unstim
LMW
MMW
HMW
Monomers
Dimers
Oligomers

381

382 **Figure 5: Highly structured β-glucans induce dimerization of Dectin-1A.**

383 (A) Representative lifetime image of HEK-293 cell transfected with Dectin-1A-mEmerald (left panel) or
384 cotransfected with Dectin-1A-mEmerald and Dectin-1A-mCherry (right panel). (B) Average lifetime of
385 HEK-293 cells expressing donor only on the cytoplasmic face, donor expressed on the cytoplasmic side
386 and acceptor on the extracellular side or donor-acceptor placed on the cytoplasmic side of the
387 membrane. Decay curves for donor only and the negative control were mono-exponentially fit while
388 cytosolic donor and acceptor decay curves were bi-exponentially fit with the first component fixed to 2.4
389 and the second component shown. Data shown as mean ± SD (n = 15 cells); Welch's t-test, ****
390 p<0.00001. (C) FRET efficiency and donor-acceptor population of cells stimulated with LMW, (D) MMW,
391 (E) HMW, or (F) DMSO denatured MMW. Data shown as mean ± SD (n = 15); One-way ANOVA multiple
392 comparisons Dunnett test, * p<0.05, **p<0.01, ***p<0.001. (G) Brightness vs intensity 2D histogram with
393 the selected pixels that contribute to the background (black), monomers (red), dimers (green), and
394 tetramers (blue) in the image. (H) Representative selection map of HEK-293 cells expressing Dectin-1A-
395 mEmerald unstimulated (left) or stimulated with MMW β-glucan (right) in which Dectin-1 aggregation
396 states are defined by colored boxes selected in the Brightness vs intensity histogram. (I) Percentage of
397 aggregates in Dectin-1A-mEmerald receptors and receptor ligand complexes obtained from N&B analysis
398 before or after stimulation. Data shown as mean ± SD (n = 30); One-way ANOVA multiple comparisons
399 Dunnett test, * p<0.05, **** p<0.00001.

400 To better characterize the aggregation states accessible to Dectin-1A, we conducted a
401 Number and Brightness analysis (N&B) on HEK-293 cells expressing Dectin-1A-
402 mEmerald. Previous research has described N&B more in depth [61–63]. Briefly, N&B
403 analysis focuses on fluctuation of detected emission photons originating from
404 fluorescent molecules that pass through a known observation volume. Statistics of fast
405 fluctuations of the intensity at each pixel can be used to determine the number and
406 intensity of the particles diffusing through the observation volume. For example, if the
407 fluorescent proteins diffuse as a tetrameric protein, we expect to observe emission

408 intensity fluctuation with four times more photons relative to a monomeric fluorescent
409 protein diffusing through the excitation volume. Receptor aggregation was observed by
410 stimulating these cells with soluble glucans. A brightness vs intensity 2D histogram of
411 each pixel in a time series was developed, and selection boxes were drawn to represent
412 monomers (red box), dimers (green box) and oligomers (blue box) (Fig. 5G). Dectin-1
413 aggregation state maps of representative untreated (Fig. 5H left panel) and MMW-
414 stimulated cells (Fig. 5H right panel) were generated using this color scheme. We
415 observed a significant increase in pixels with a dimer and oligomer brightness in cells
416 stimulated with MMW and HMW compared to cells that were unstimulated or LMW
417 stimulated (Fig. 5I). N&B analysis revealed that dimers of Dectin-1A account for the
418 majority of aggregated state Dectin-1.

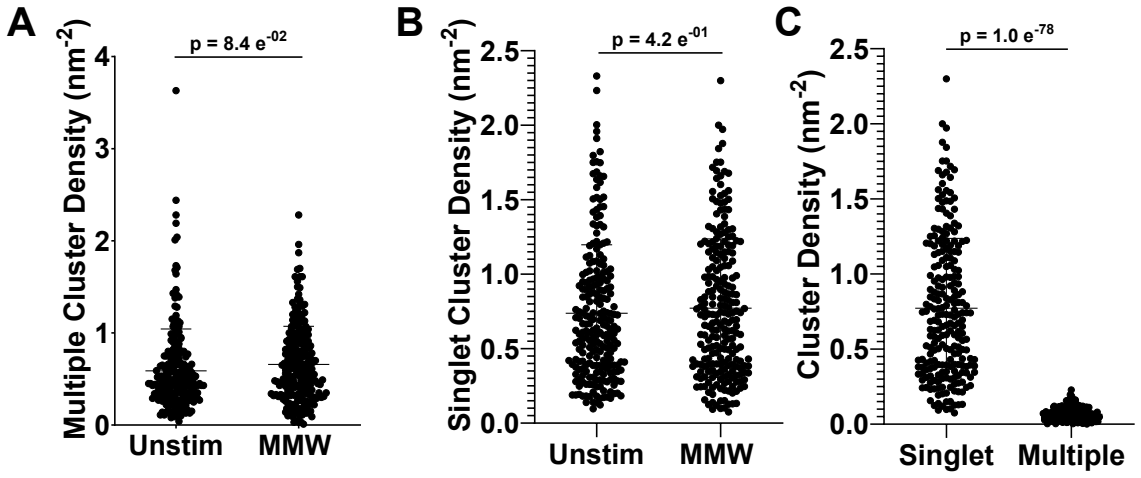

419

420 **Figure 6: Dectin-1A does not form large scale aggregation when stimulated with**
421 **highly structured β-glucan.**

422 (A) Multiple cluster density of dSTORM analysis of HEK-293 cells expressing Dectin-1A unstimulated or
423 stimulated with MMW. A singlet cluster is a cluster of localizations determined to arise from 3 or more

424 individual Dectin-1 proteins. (B) Singlet cluster density of DSTORM analysis of HEK-293 cells expressing
425 Dectin-1A unstimulated or stimulated with MMW. A singlet cluster is a cluster of localizations determined
426 to arise from a single Dectin-1 protein, or potentially >1 Dectin-1 protein within sub-resolution
427 displacements from one another. (C) Density of singlet and multiple cluster of Dectin-1A expressing HEK-
428 293 cells treated with MMW. Data shown as mean ± SD (n = 34) with significance assessed by Student's
429 t Test.

430

431 **β-glucan induced Dectin-1A aggregates are below 15 nm in size**

432 While FRET-based observations and N&B analysis clearly show the presence of ligand-
433 induced, molecular-scale aggregation (e.g., dimerization) of Dectin-1A, these methods
434 are not as well suited to discern the existence of larger scale aggregation of the
435 receptor (e.g., clusters of tens to hundreds of receptors). We used direct Stochastic
436 Optical Reconstruction Microscopy (dSTORM) coupled with Hierarchical Single-Emitter
437 hypothesis Test (H-SET) analysis [13] to resolve aggregation of Dectin-1A before and
438 after stimulation with MMW glucan. This localization super resolution microscopy
439 technique accurately resolves objects from the diffraction limit (~300 nm, the resolution
440 limit of conventional fluorescence microscopy methods) or above, down to ~15 nm (a
441 typical resolution limit of dSTORM using our configuration). H-SET analysis detected
442 sites of Dectin-1 labeling as "singlet" objects or "multiple" clustered objects. Multiple
443 clustered objects are those with three or more resolvable individual Dectin-1 molecules.
444 Singlet objects are those that appear to contain only a single, resolvable Dectin-1
445 labeling event, though it is possible that multiple Dectin-1 molecules in very close
446 proximity (<15 nm separation) would be unresolvable and appear as a singlet object.
447 We detected no significant change in the density of singlet objects or multiple object

448 clusters before vs after MMW glucan stimulation (Fig. 6A,B; Supplemental Fig. 1).
449 Consistent with our previous findings, singlet exposures greatly outnumber multiple
450 exposures on the cell wall surface (Fig. 6C). Localization number per multiple cluster
451 object did not change with stimulation (Supplemental Fig. 1), suggesting no change in
452 the number of receptors in such objects. Ripley's K analysis suggests clustering up to
453 the ~50 nm length scale but not at longer length scales (Supplemental Fig. 1). In the
454 context of the previous findings showing molecular aggregation at very small scales,
455 potentially below the resolution limit of dSTORM, we concluded that dSTORM results
456 indicated that the Dectin-1A aggregates formed upon glucan stimulation are quite small
457 and below the resolution limit of dSTORM (<15 nm length scale). Because this places
458 an upper bound on the size of ligand-induced Dectin-1 clusters and we can estimate
459 that the CRD of Dectin-1 occupies an area approximately 25 nm^2 (PDB: 2BPD; [58,64]),
460 we conclude that Dectin-1 aggregation after MMW glucan stimulation most likely
461 involves collections of not more than ~7 receptors.

462 **Dectin-1A is predominantly monomeric in resting cell membranes**

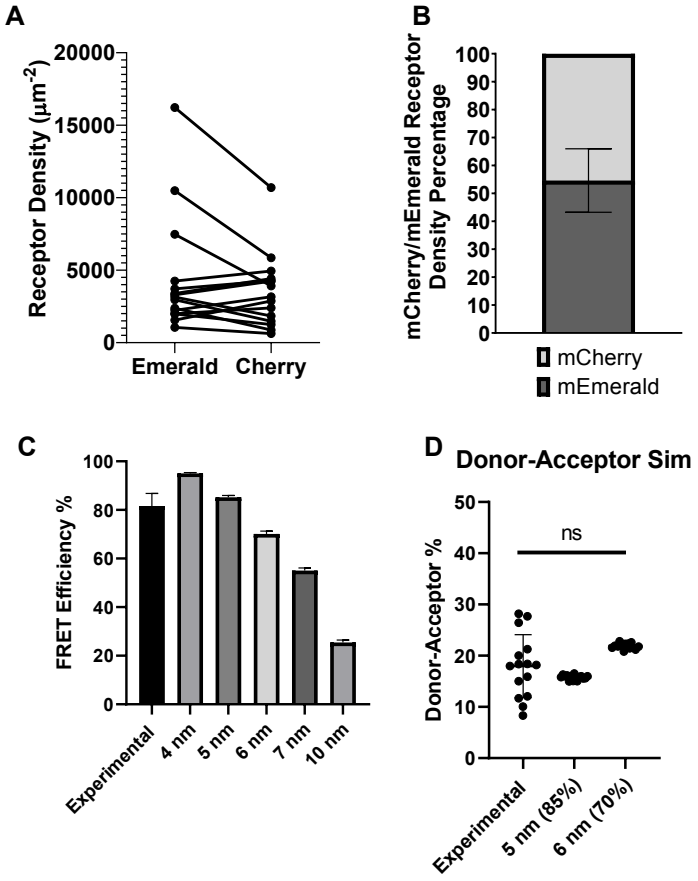

Figure 7 Dectin-1A collisional diffusion FLIM-FRET model:

(A) Receptor density of HEK-293 cells co-expressing Dectin-1A-mEmerald and -mCherry. (B) Ratio of mEmerald/mCherry expression in unstimulated HEK-293 cells. (C) FRET Efficiency (FE) of Dectin-1A donor/acceptor simulated at different maximum intermolecular radial distances and experimental observations of FRET in resting cells. (D) Percentage of donors undergoing FRET (Donor-Acceptor Population) for experimental results from resting cells and FLIM FRET simulations at 5 and 6 nm maximum radii. Data shown as mean ± SD (n = 15 independent simulations or experimental observations on cells, respectively); One-way ANOVA multiple comparisons Dunnett test.

473 FRET-based measurements and N&B analysis reported that the large majority of
474 Dectin-1 is distributed as monomers in unstimulated cells. However, a minority
475 population of receptors in states indicative of some close intermolecular interaction was
476 observed in these cells by both techniques. This may represent random collisional
477 interactions between Dectin-1 molecules, with no stable receptor oligomer formation.
478 For instance, FRET may be observed from random collisional interactions without
479 requiring stable receptor aggregation. Alternatively, it is possible that a small fraction of
480 Dectin-1 does form dimers or oligomers, even in the absence of glucan. It is difficult to
481 conclusively distinguish between these alternative hypotheses using only the
482 experimental results shown above. Therefore, we created a computational model of fully
483 monomeric Dectin-1 undergoing Brownian 2D diffusion to predict FLIM-FRET results
484 anticipated from a purely monomeric receptor system. We determined the receptor
485 density of both donor and acceptor for HEK-293 cells coexpressing Dectin-1A
486 mEmerald/mCherry by RICS analysis (Fig. 7A). Our results indicated on average
487 Dectin-1 co-transfected cells contain 54.6% mEmerald and 45.4% mCherry (Fig. 7B).
488 Therefore, our model was populated by equal proportions of donor and acceptor tagged
489 Dectin-1 molecules. Their diffusion coefficients were parameterized using data from Fig.
490 4. The model calculated FRET rates for all donor-acceptor pairs within a specified
491 maximum radial distance. The maximum radius for experimental FRET observation is
492 limited by signal-to-noise ratio and other factors. To avoid simulating FRET
493 measurements at experimentally unrealistic radii, we varied the maximum donor-
494 acceptor radial distance in a range of 4-10 nm and constrained the model with an
495 experimentally realistic maximum radius for calculation of FRET. We compared

simulated and experimental FRET efficiencies and used maximum radii for simulation that yielded FRET efficiency in best agreement with observed FRET efficiency on resting cells. Our results show our experimental FRET efficiency values match model predictions closely at maximum radii between 5 and 6 nm (Fig. 7C). Simulations at these radial parameters were then compared to experimental results with respect to the donor-acceptor population percent that they predicted.

We used the predictions of this computational model to test the hypothesis that random collisional FRET interactions of donors and acceptors is sufficient to explain the basal FLIM-FRET signal observed experimentally in resting cells. If this model, which incorporates only collisional interactions between donors and acceptors, predicts a percent of donors undergoing FRET interactions with acceptors that matches the experimentally observed value, we would consider that collisional interactions alone are sufficient to explain the observed basal FRET signal. However, if the model predicts a value significantly below that experimentally observed, we would propose that a minor fraction of Dectin-1 molecules may participate in aggregates on cell membranes, even in the absence of glucan. Using simulations with radial values of 5 and 6 nm, our results indicate that the experimentally observed amount of Dectin-1 receptors participating in FRET interactions (Donor-Acceptor population) prior to stimulation match closely to our simulated results (Fig. 7D). This indicated that the FRET signal we observe prior to stimulation was attributable to random collisional interactions of monomerically diffusing receptor expected at the Dectin-1A expression level present in our experimental system.

519 **Dectin-1A dimer/oligomer and contact site formation is more efficient with cells**
520 **incubated with *C. albicans* containing high glucan exposure.**

521 Throughout the article, we have focused on experiments using soluble glucans. In order
522 to show Dectin-1 aggregation occurs during fungal cell recognition, we used high
523 (TRL035) and low (SC5314) β-glucan exposing *C. albicans* strains and examined
524 Dectin-1 aggregation occurring at the contact sites with these yeast. TRL035 has been
525 previously shown to have high glucan exposure compared to SC5314 [65]. In addition,
526 our representative images show TRL035 forming a phagocytic cup more efficiently then
527 SC5314 (Fig. 8A). We observed no significant difference in FRET efficiency between
528 any conditions tested (Fig. 8B), similarly to our observations with soluble glucan. This
529 finding is consonant with a larger trend in the data presented in this report where FRET
530 efficiency is relatively constant and differences in glucan recognition seem to be mainly
531 associated with differences in the proportion of Dectin-1A molecules engaged in
532 molecular aggregates. Our results further show that HEK-293 cells co-transfected with
533 Dectin-1A-mEmerald and Dectin-1A-mCherry exhibit an increase in the proportion of
534 aggregated-state receptors from approximately 15% in non-contact site membrane to
535 about 25% in contact sites of high glucan exposing yeast TRL035 and glucan particles
536 (Fig. 8C). Interestingly, we did not measure a significant increase in receptor
537 aggregation between non-contact membranes and contact sites with low glucan
538 exposing SC5314. The significance and interpretation of these findings is further
539 discussed below. These results suggest that larger glucan exposure results in an
540 increase of Dectin-1 in molecular aggregates with associated signaling, resulting in a
541 more efficient recognition of yeast by the Dectin-1A receptor.

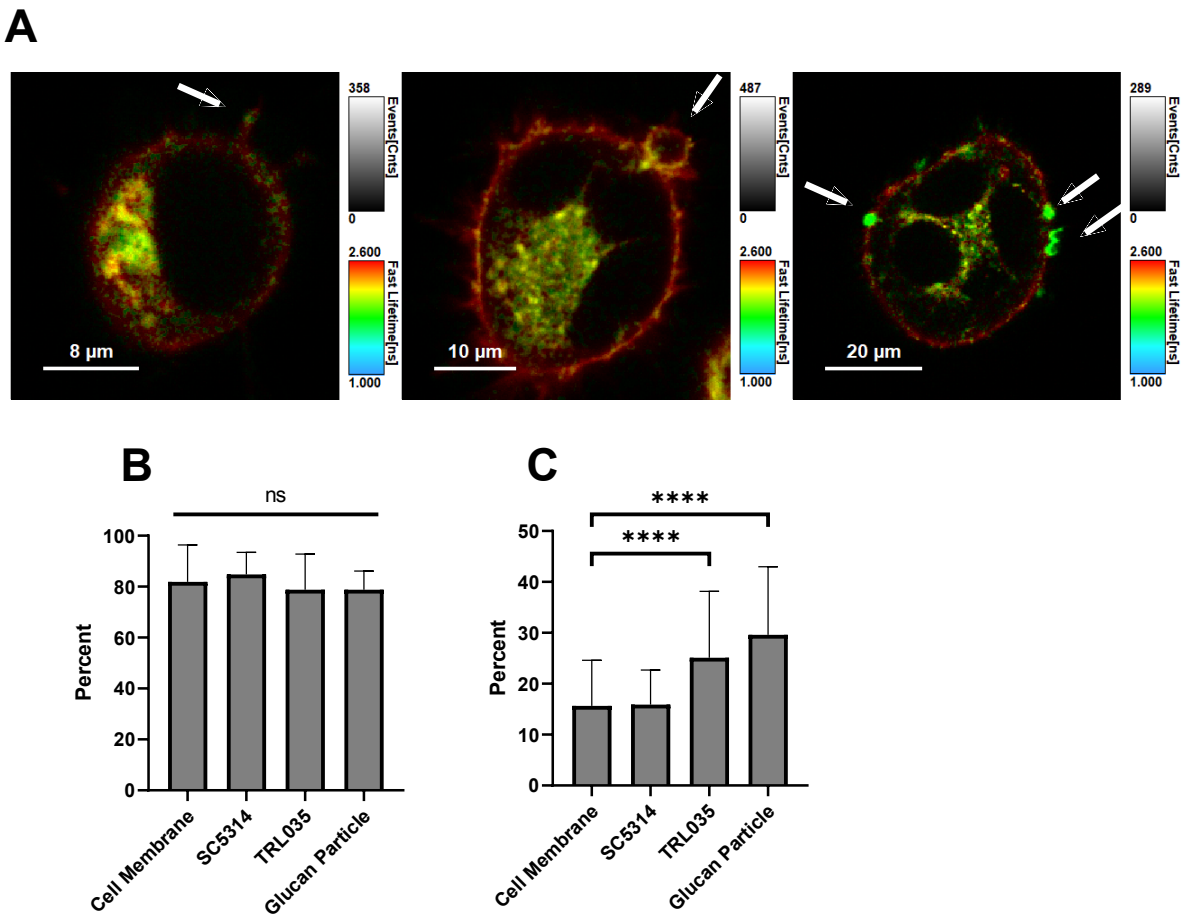

Figure 8: Dectin-1A forms more oligomers at fungal contact sites with high β-glucan exposure.

(A) Representative lifetime images of HEK-293 cells co-transfected with Dectin-1A-mEmerald and Dectin-1A-mCherry incubated with SC5314 (left panel), TRL35 (middle panel) or particulate glucan (right panel). Transition from redder to greener pixels at contact sites is indicative of increased FRET interactions between Dectin-1 receptors. (B) FRET efficiency and (C) donor-acceptor population of cell membranes with no fungal contact, SC5314 (low glucan exposure), TRL35 (high glucan exposure), or particulate glucan. Data shown as mean ± SD (n = 15); One-way ANOVA multiple comparisons Dunnett test, **** $p<0.00001$.

553 **Discussion**

554 Our results demonstrate that the structure of β-glucan impacts receptor signaling by
555 determining the membrane organization and molecular aggregation state of Dectin-1A.
556 We showed that glucans with higher order structure are better able to activate Dectin-
557 1A signaling. Upon activation by stimulatory soluble glucan, Dectin-1A enters
558 aggregated states that contain dimers and higher order oligomers, but these appear to
559 remain as small nanoscale domains containing relatively small numbers of receptors.
560 Comparison of computational modeling and experimental FLIM-FRET data confirms
561 that Dectin-1A exists in a monomeric state in resting cells. Further, monomeric
562 receptors oligomerize and aggregate in a fashion that is dependent upon glucan higher
563 order structure and correlated with the magnitude of membrane proximal signaling
564 downstream of Dectin-1. Finally, we observed that a similar process of increasing
565 Dectin-1 aggregation is seen at contact sites with yeast and fungal-derived particles,
566 and the amount of aggregated state Dectin-1A correlates with the degree of glucan
567 exposure on the surface of the particle. We have summarized all of our quantitative
568 findings in numerical form in Supplemental Table 3 for convenient reference.

569 β-glucan is widely distributed on various fungal species as an insoluble component of
570 the cell wall. The soluble form is produced when macrophages recognize fungal
571 surfaces and release enzymes that degrade cell wall glucans [47,48]. These soluble
572 glucans are commonly found in circulation in the serum of patients with fungal infections
573 [49,50]. β-glucans possess three different structures: low molecular weights possess a
574 random coil structure while high molecular weight glucans possess either a single or
575 triple helical structure [66]. Furthermore, studies have shown that the complexity of β-

576 glucan is associated with stronger immunostimulatory effects [17,27,29,66,67].
577 However, these ensemble-based studies concern β-glucan stimulation at the population
578 level. Therefore, we took a single cell approach to understand nanoscale glucan
579 signaling dynamics using glucans that vary in size and structure. In line with previous
580 studies, our results revealed that Dectin-1A activation is influenced by the β-glucan
581 triple helical structure. Together, these findings demonstrate that β-glucan impacts
582 receptor signaling due to structure and not merely through its affinity or size.

583 A previous study indicated that the amount of glucan triple helical structure positively
584 correlates with its binding affinity for receptors on human promonocytic cells, and
585 biochemical evidence suggested that glucans with more triple helical content exhibit
586 greater selectivity in receptor interactions on these cells [27]. This evidence suggests
587 that glucan higher-order structure does impact the character of ligand-receptor
588 interactions in the context of whole cells. We hypothesized that glucan structure
589 impacts signaling by modulating the frequency of Dectin-1A dimer/oligomer formation,
590 thus creating sites where Syk could be better recruited via interactions of its SH2
591 domains with the phosphorylated YXXL sequence in the Dectin-1A cytosolic tails. Our
592 FLIM-FRET results reveal that Dectin-1A enters a state of greater molecular
593 aggregation when stimulated with β-glucans possessing higher ordered helical
594 structure. These results agree well with a previously described model of (hem)ITAM
595 signaling from another C-type lectin receptor, CLEC-2, in which the minimum signaling
596 unit for CLEC-2 is a phosphorylated dimer, enabling recruitment of a single molecule of
597 Syk [45].

598 In addition, our FLIM-FRET results suggested possible intermolecular interactions
599 between Dectin-1 proteins even before stimulation with β-glucan. We considered this
600 possibility carefully because receptor oligomeric states exist in the basal state for some
601 other C-type lectin receptors, such as DCSIGN, DNGR-1, and NKp80 [68–71].
602 However, Dectin-1A does not contain cysteine residues in its stalk region which have
603 been shown to be important in the dimerization of other C-type lectin receptors.
604 Therefore, it is considered that Dectin-1A, like CLEC-2, is more likely to experience
605 ligand-induced aggregation in the form of non-disulfide-linked homodimers instead [70–
606 72]. Our experimental data did show evidence of close molecular interactions between
607 individual Dectin-1A proteins in the membrane, but comparison with modeling results
608 indicates that this signal is attributable to an expected level of very transient collisional
609 interactions between the receptors, given the receptor density and diffusion coefficient
610 present in our experimental system. Therefore, our membrane biophysical
611 investigations are most consistent with a model wherein transient Dectin-1A interaction
612 events may occur in resting cell membranes, but upon ligation by highly structured
613 glucans, dimers and small oligomers are stabilized, which drives increased efficiency of
614 Dectin-1 signaling.

615 Throughout our experimental FLIM-FRET datasets, we repeatedly observed significant
616 glucan induced shifts in the percentage of donors that were participating in FRET
617 interactions, but little change in FRET efficiency as a function of glucan stimulation.
618 FRET efficiencies measured were relatively constant across experimental conditions
619 and also quantitatively fairly high (typically about 75-85%). This suggests that when
620 FRET was experimentally observed, it was derived from close intermolecular

621 interactions of neighboring Dectin-1A molecules, such as might be expected in an
622 ordered molecular aggregate, such as a dimer or tetramer. In such an aggregate,
623 donor-acceptor separation distances are not free to vary over a wide range because,
624 while the aggregate state exists, those distances are determined by the ordered
625 structure of the protein-protein complex. Therefore, we think that our data is consistent
626 with a model wherein Dectin-1 transitions between monomeric forms and ordered
627 intermolecular aggregate states. We observe that glucan structure controls Dectin-1
628 aggregation primarily by changing the fraction of receptors in aggregated states.

629 Similarly, our N&B results indicate a formation of dimers and oligomers in cells
630 stimulated with glucans possessing significant higher order helical structure. These
631 findings are directly in line with previous crystallographic studies that show monomeric
632 Dectin-1A CRD in the absence of glucan but able to form dimeric complexes in the
633 presence of β-glucan [58]. In addition, other studies have shown a ligand-induced
634 cooperative formation of Dectin-1 CRD tetramers [59]. However, these studies were
635 performed with truncated receptor ectodomain proteins outside the context of living cell
636 membranes, so our findings better establish and define the relevance of such ordered
637 aggregate states to full length Dectin-1 in a more physiologically realistic context.

638 Our dSTORM super resolution results indicate a lack of large aggregates forming.
639 Because of the resolution limit of 15 nm, it is possible that our dSTORM analysis is
640 limited in its ability to resolve the formation of small aggregates. Furthermore, it is also
641 possible that in the soluble form, receptors are internalized rapidly, not allowing for
642 plasma membrane aggregate formation to be observed. In the case of glucan
643 encountered at the yeast cell wall, Dectin-1 aggregates may form at the host-fungal cell

644 contact site, where engaged receptor is physically prevented from quickly internalizing.
645 A previous work demonstrated the organized recruitment of Dectin-1 to a “phagocytic
646 synapse” with glucan particles, where Dectin-1A interactions were presumed to occur
647 and give rise to signaling [73]. Our study directly demonstrates the aggregation of
648 Dectin-1 at these surface interaction sites in living cells. In the future, these studies may
649 be expanded to better characterize the dynamics of receptor recruitment, aggregation
650 and internalization at phagocytic synapses with fungal pathogens.

651 To determine if this phenomenon occurs at early time points of fungal recognition, we
652 conducted FLIM-FRET experiments of contact sites of *C. albicans* lab strain SC5314
653 and our clinical isolate TRL035. TRL035 has been previously described as having
654 higher glucan exposure compared to SC5314 due to a 3-fold reduction of mannan
655 structure [65]. Our results indicate an increase in Dectin-1A aggregation at the contact
656 sites of yeast that have higher glucan exposure as well as contacts with particulate
657 glucan. We were only able to observe increases in contact site Dectin-1A aggregation
658 state for yeast and fungal particles with unusually high glucan exposure for *C. albicans*
659 yeast. No such increase over non-contact membrane sites was detectable at contact
660 sites with SC5314 *C. albicans* yeast (low glucan exposure due to efficient glucan
661 masking). This observation does not necessarily imply that there is no Dectin-1
662 aggregation in response to glucan exposures on *C. albicans* SC5314. The fraction of
663 Dectin-1 in aggregated states vs the monomeric state may be small enough to be below
664 our limit of detection by FLIM-FRET in this case.

665 Glucan exposure magnitude is thought to be regulated by masking of glucan by outer
666 cell wall mannoproteins, providing a very effective mechanism of fungal immune

667 evasion in *C. albicans*. Our previous optical nanoscopy studies of glucan exposure on
668 *C. albicans* SC5314 and TRL035 have revealed a severely limited cell wall surface area
669 containing exposed glucan that is capable of multivalent interaction with Dectin-1. It is
670 reasonable to presume that these limited sites of multivalent glucan exposure may be
671 the rate limiting factor in determining Dectin-1 aggregation and signaling at phagocytic
672 synapses. Our previous studies allow us to estimate multivalently-engaging glucan
673 exposure site density and area (per exposure site) as follows: SC5314—1 μm^{-2} density,
674 6.61×10^{-4} μm^2 area; TRL035—4 μm^{-2} density, 9.62×10^{-4} μm^2 area [65]. We previously
675 measured the total area of contact sites between *C. albicans* and human immature
676 dendritic cells as ~10 μm^2 [74]. Finally, we have estimated (see above) that one Dectin-
677 1 CRD occupies a footprint of ~25 nm^2. From these figures, we can estimate that one
678 typical 10 μm^2 phagocytic synapse would contain a maximum of ~264 multivalently
679 engaged Dectin-1 proteins for *C. albicans* SC5314, and maximum ~385 multivalently
680 engaged Dectin-1 for TRL035. For comparison, at the observed receptor density in our
681 model (Fig. 4), we would expect ~46000 total Dectin-1 proteins to be present in this
682 entire phagocytic contact membrane. However, an important caveat is that, in our model
683 system, we noted that SC5314 phagocytic synapses were much smaller than those for
684 TLR035. A smaller contact site would reduce the number of multivalently engaged
685 receptors in SC5314 synapses considerably relative to the above estimates—perhaps
686 decreasing the number of multivalently engaged Dectin-1s by approximately an order of
687 magnitude. So, these estimates emphasize Dectin-1 system is highly sensitive and able
688 to drive signaling responses when only a few hundred receptors, corresponding to less
689 than 1% of the total contact site resident Dectin-1 proteins, are aggregated in the

690 phagocytic synapse. Moreover, these results and estimates suggest that fungal
691 recognition requires the Dectin-1 system to engage in a search for rare sites of
692 multivalent interaction with glucan. It is very likely that Dectin-1 must cooperate with
693 other anti-fungal receptors for the purposes of building and stabilizing the fungal contact
694 wherein this search process operates. This aspect of receptor cooperativity is an
695 aspect of fungal recognition not present in our simplified experimental model. Future
696 studies may productively address how other CTLs (i.e., DC-SIGN and CD206, which
697 establish firm adhesion to abundant fungal surface mannans) may physically and
698 biochemically assist in Dectin-1's search for rare ligand by building and maintaining a
699 robust phagocytic synapse.

700 Previous research has shown that glucan unmasking can be caused by enzymatic
701 degradation of the mannoproteins by macrophages after initial recognition of the fungal
702 cell [47,48]. Furthermore, anti-fungal drugs have also been shown to unmask fungal cell
703 walls that then allow for clearance by the host's immune system [13,14]. Our previous
704 studies have shown that the vast majority of cell wall glucan exposures are only large
705 enough to engage a single Dectin-1 CRD, suggesting that most glucan exposures may
706 not be able to multivalently engage Dectin-1. The fact that most glucan exposure sites
707 on SC5314 *C. albicans* yeast are of this type may explain why we are not able to see
708 much Dectin-1A aggregation in their contact sites. In contrast, we have reported that
709 TRL035 has an increased density and size of glucan exposures capable of multivalent
710 Dectin-1 interactions, which agrees with our finding of increased molecular aggregation
711 of Dectin-1A at contact sites with TRL035 in the present study. Overall, our findings
712 have been consistent with a model wherein the ability of Dectin-1 to find and aggregate

713 at multivalent exposures of glucan on fungal cell wall surfaces is a critical determinant of
714 Dectin-1 dependent innate immune fungal recognition.

715 Overall, these findings indicate that β-glucan structure is required for Dectin-1A to
716 undergo Syk-dependent signaling. Here we provide evidence in support of a model in
717 which highly structured glucans induce dimerization and/or oligomerization of the
718 receptor. This allows their (hem)ITAM domains to become close enough to allow for the
719 activation of Syk, leading to further signaling cascades. Greater understanding of
720 receptor activation is required to better understand the role of Dectin-1A and its agonists
721 as a potential way forward for adjuvant and immunotherapy development. Furthermore,
722 given the worldwide burden of candidiasis, further experimentation is required to better
723 understand the role of Dectin-1A in recognition of these pathogens.

724

725 **Materials and Methods:**

726 **Cell Culture**

727 The HEK-293 (ATCC, #CRL-1573) cell line was maintained in Dulbecco's minimum
728 essential medium supplemented with 10% Fetal Bovine Serum (FBS), 1%
729 penicillin/strepromycin, 2mM L-glutamine, 11mM Sodium pyruvate, and 1% HEPES.
730 Cells were maintained in an incubator at 37°C at 5% CO_2 levels. Cells were maintained
731 at 37°C, 5% CO_2, and 75% humidity during imaging.

732 **Plasmid**

733 Emerald-Dectin1A-N-10(Addgene plasmid, #56291), Emerald-Dectin1A-C-10 (Addgene
734 plasmid # 54057), mCherry-Dectin1A-C-10 (Addgene plasmid # 55025), and mCherry-
735 Dectin1A-N-10 (Addgene plasmid # 55026) was a gift from Michael Davidson.
736 Transfection with plasmids was performed using standard protocols of Fugene 6
737 (Promega, #E2691). pUNO1-hDectin-1A (Invivogen) was stably transfected into HEK-
738 293 cells for use in our calcium studies. HEK-293 cells were selected using Geneticin
739 (G418 Sulfate) (Thermo-Fischer, #10131035) at 400 ug/ml for 2 weeks.

740 **Fungal Growth/Preparation**

741 *C. albicans* SC5314 (ATCC, MYA-2876) or TRL035 yeast cells were grown from
742 glycerol stock, stored at −80°C. Samples were grown in YPD, for 16 h at 37°C in an
743 orbital shaker at 250 rpm to mid log phase. Following a 3-minute centrifugation at 6000
744 rpm, the supernatant was removed, and the cells were resuspended in 4%
745 paraformaldehyde and sterile phosphate-buffered saline (PBS) for 15 minutes. The cells
746 were centrifuged and washed with sterile PBS 3 times. The cell concentration was then
747 determined using a disposable hemocytometer (C-Chip; Bulldog Bio catalog no. DHC-
748 N01). 3.5 x10^6 cells were resuspended in 1 ml of PBS. 100 µl of the solution was added
749 to HEK-293 cells in 35 mm dishes 15 minutes prior to imaging.

750 **Soluble Glucans Chromatographic Analysis**

751 Low (LMW, 11 kDa), medium (MMW, 145 kDa), and high (HMW, 450 kDa) molecular
752 weight β-1,3;1-6-glucan extracted from *S. cervisiae* cell wall was generous gift from
753 ImmunoResearch Inc. (Eagan, MN). The molecular weight was assessed by gel
754 permeation chromatography (GPC) and multi angle light scattering (MALS). Samples

755 (100 µg) were injected and eluted with a mobile phase of 0.15 M sodium chloride
756 containing 0.02% sodium azide at a flow rate of 0.5 mL/min using two Waters
757 Ultrahydrogel 500 columns and one Waters Ultrahydrogel 250 column connected
758 serially. The samples were run with the column temperature at 18°C. The Mw was
759 calculated using Wyatt Astra software using data resulting from measurements of the
760 angular variation of scattered light using the MALS detector coupled with the
761 concentration measured by the DRI signal.

762 **Soluble Glucan Linkage Analysis**

763 Desalted and lyophilized samples of the fractions were dissolved in dimethylsulfoxide
764 (DMSO) and treated with NaOH and methyl iodide to methylate all free hydroxyl groups
765 [75]. The methylated material was purified by extraction with dichloromethane and
766 washing with water. The purified material was then hydrolyzed with trifluoroacetic acid,
767 the reducing ends of the resulting sugars were reduced with $NaBD_4$, and then the
768 resulting free hydroxyl groups were acetylated with acetic anhydride. The mixture of
769 partially methylated alditol acetates was analyzed by gas chromatography. Each
770 derivative corresponding to a particular linkage has been identified by a characteristic
771 retention time and mass spectrum using a mass detector. The relative amount of each
772 derivative was measured by gas chromatography with flame ionization detection. The
773 areas obtained for each observed peak are used to calculate the relative amounts of
774 each type of linkage found in the sample (Table 1). The 3,6-linked residues represent
775 branch points.

776 **Table 1.**

	LMW	MMW	HMW
Terminal Glucose	6.4	5.1	5.4
3-Glucose	87.5	87.6	84.6
3,6-Glucose	3.2	3.8	4.0
6-Glucose	1.3	2.2	3.2
4-Glucose	0.1	0.2	0.1
Other	1.5	1.1	2.7

777

778 **Soluble Glucan ^{1}H NMR Spectroscopy**

779 The samples were dissolved in DMSO-d6/D2O (6:1 by volume) at 100°C for 1 h.
780 ^{1}HNMR Spectra were recorded at the University of Minnesota Department of Chemistry
781 NMR lab on a Varian UNITYplus-300 spectrometer at 80°C. The spectra were collected
782 at 300 MHz with 32 scans, a relaxation delay of 1.5 seconds, a pulse of 45°, an
783 acquisition time of 2.0 seconds, and a spectral width of 5999 Hz. Table 2 provides ^{1}H
784 NMR chemical shifts in all three glucans used in this study as well as literature values
785 [76]. These data, taken together with other characterization methods used, do confirm
786 that the structure of the polysaccharides used in this study conforms to expected results
787 from fungal cell wall glucans (Table 2, Supplemental Fig. 2).

788 **Table 2.**

	H-1 (1,3-glucan)	H-2, 4, and 5 (1,3-)	H-3 and 6b (1,3-)	H-6a (1,3-)
LMW	4.52, d, J = 7.8 Hz, 1H	3.20-3.33 m, 3H	~3.5, m, (hidden by H_2O)	3.72, d, J = 11 Hz, 1H
MMW	4.52, d, J = 8.1 Hz, 1H	3.21-3.33 m, 3H	~3.5, m, (hidden by H_2O)	3.72, d, J = 11 Hz, 1H
HMW	4.52, d, J = 7.8 Hz, 1H	3.20-3.32 m, 3H	~3.5, m, (hidden by H_2O)	3.72, d, J = 11 Hz, 1H
Beta 1,3/1,6 Glucan Literature values	4.52, d, J = 8 Hz, 1H	3.25, m, 3H	3.46, m, 2H	3.7, d, J = 11 Hz, 1H

Particulate Glucan

Particulate beta-glucan was prepared from a lyophilized pellet of C. albicans SC5314 yeast. These were boiled in 0.75M NaOH for 15 min, residue was collected, and two additional rounds of the identical treatment were applied. The residue was boiled for 15 min in 2M phosphoric acid, residue was collected and two additional rounds of the identical treatment were applied. The residue was extracted in ethanol with 1% phosphoric acid by boiling for 15 min, residue was collected, and two additional rounds of the identical treatment were applied. The residue was neutralized to pH 7.0, boiled in

809 water for 15 min, residue was collected, and two additional rounds of the identical
810 treatment were applied. The suspension of glucan microparticles was predominantly
811 monodisperse and stored in sterile water at 4C. Depyrogenated glassware and
812 endotoxin free reagents were used in the preparation of glucan particles.

813

814 **Microscopy and Image Analysis**

815 Confocal images were obtained on an Olympus FV1000 laser scanning confocal
816 microscope (Olympus, Center Valley, PA) built around an IX81 inverted microscope.
817 Temperature and CO_2 was controlled at 37°C and 5% respectively. A 10x objective lens
818 (0.40 NA) and a super corrected 60X oil objective lens (1.40 NA), Plan-Apochromat
819 objective lens was used for imaging. Samples were excited with a 473 nm diode laser
820 and a 20 mW, 635 nm diode laser. These lines were reflected to the specimen by a
821 405/473/559/635 multi-edge main dichroic element followed by bandpass emission
822 filters in front of 2 independent High sensitivity GaAsP PMT detector (HSD1/2).
823 Specifically, the emission light passed by the main dichroic was directed to our first
824 detector (HSD1) via SDM560 filter cube and passage through a BA490-540 nm
825 bandpass filter. Our second detector (HSD2) received light from SDM560 filter cube to
826 BA575-675 nm bandpass filter.

827 **Fluo-4 Calcium Imaging**

828 HEK-293 cells expressing Dectin-1A were plated at 40,000 cells in a 35 mm (MatTEK
829 dishes) 24 hours prior to imaging. These cells were loaded with Fluo-4 and Cell Mask
830 Deep Red (CMDR) at equimolar concentrations of 1 μM in 2 mLs of media for one hour

831 then washed before imaging. Cell Tracker Deep Red was used as a cell cytosolic
832 volume control to account for cytosolic changes from cell contraction that occurs during
833 stimulation. For Syk inhibition, plates were treated with 250 nM of Syk Inhibitor (Calbio
834 chem, #574711) as per the company's specifications. Images were taken at a resolution
835 of 256 x 256 with a dwell time of 2 μs on a 10x objective lens (0.40 NA). A 20 mW, 473
836 nm diode laser operated at 4% power and CMDR was excited with a 20 mW, 635 nm
837 diode laser operated at 4% power. Fluorescence of Fluo-4 was collected by a cooled
838 GaAsP PMT set to 700V, gain 1X and offset of 0%. Our CMDR was collected through
839 our by a cooled GaAsP PMT detector set to 700V, gain 1X and offset of 0%. 30 frames
840 prior to stimulation were used to set the basal fluorescence of the fluo-4 dye. After
841 stimulation with 100 μl of 10ug/ml of glucan, cells were imaged for 100 frames. To
842 assess changes in intracellular calcium concentration, we measured the ratio of Fluo-
843 4/CMDR intensity in order to correct for any variations in cytoplasmic volume within the
844 confocal section across the field. This ratio was normalized to 1.0 based on mean pre-
845 stimulation values (30 frames) and changes in calcium influx were measured as fold
846 change of this normalized ratio (MFI fold change).

847 For MMW denaturation experiments, soluble β-glucans were weighed and resuspended
848 in reverse osmosis purified H_2O. In order to denature medium molecular weight glucan,
849 we incubated MMW in DMSO or 1M NaOH. To renature the glucan from DMSO, we
850 placed denatured MMW into Slide-A-Lyzer Dialysis Cassettes (Catalog no. 66203) of a
851 molecular weight cut-off of 2,000 Da and dialyzed against reverse osmosis purified H_2O
852 for 24 hours. To renature glucan from 1M NaOH, the solution was neutralized using 1M
853 HCl.

854 **Protein isolation and immunoblotting**

855 HEK-293 cells stably expressing mEmerald-Dectin-1A were seeded at 5 x 10^5 in 6-well
856 plates 24 hours prior to the experiment. Cells were stimulated with Low, Medium and
857 High molecular weight β-glucan with 1 mg/ml for 5 minutes then lysed. Cells were
858 extracted in 1X lysis buffer (43.9mM HEPES, pH 7.5; 131.7mM NaCl; 1.1% Triton X-
859 100; 8.8% glycerol; 1x protease inhibitor cocktail; 1mM PMSF; 1mM EGTA). Samples
860 were centrifuged at 12,000g for 20 min at 4°C and supernatants transferred to fresh
861 tubes. Protein concentrations were determined by Bradford assay (Bio-Rad Protein
862 Reagent). NuPAGE LDS sample buffer (4X) with NuPAGE Sample Reducing agent
863 (10X) was added to samples (1X final concentration). Total proteins (typically 20-50 µg)
864 were subjected to 4-12% sodium dodecyl sulfate-polyacrylamide gel electrophoresis
865 (SDS-PAGE). Proteins were transferred to Immobilon-FL PVDF transfer membrane
866 (Millipore Sigma) using NuPAGE transfer buffer. Membranes were blocked with bovine
867 serum albumin in Tris-buffered saline-Tween-20 (TBS-T; 20 mM Tris, 137 mM NaCl,
868 0.1% Tween-20) and incubated with primary antibodies overnight at 4°C. Antibodies
869 purchased from Cell Signaling: Rabbit mAb for p-SYK (Tyr525/526) and β-Actin (13E5),
870 and mouse mAb Syk (4D10) were used according to manufacturer's recommendations
871 (1:1000). HRP-conjugated anti-mouse and anti-rabbit secondary antibodies (Cell
872 Signaling or GE Healthcare) were used at a 1:10,000 dilution. Blots were visualized on
873 a Li-Cor Odyssey FC imaging system and analyzed with Image Studio.

874 **Biolayer interferometry**

875 Advanced Kinetics Biolayer interferometry experiments were conducted using the
876 Personal Assay BLItz System. Anti-human IgG Fc Capture (AHC) Biosensors tips were

877 initially loaded with Dectin-1A:FC fusion protein (Invivogen, #fc-hdec1a) at 13 ug/ml.
878 Binding kinetics were obtained for LMW, MMW, HMW, MMW (denatured) and MMW
879 (renatured) at 0, 10, 50,100, and 250 nM in triplicate. A global fitting was performed on
880 the curves obtained using the BLItz software.

881 **Congo Red Assay for Glucan Structure**

882 A BioTek EON Multiwell Spectrophotometer was used to analyze Congo Red
883 absorbances. A solution of 8.8 μM Congo Red, 0M-1M NaOH solution (1 M, 0.75 M, 0.5
884 M, 0.25 M, 0.1 M, 0.075 M, 0.05 M, 0.025 M, 0.001 M, 0 M) and LMW, MMW, or HMW
885 β-glucans at 1 mg/ml were analyzed for the denaturation experiments. For the
886 renaturation experiments, 1mg/ml of β-glucan was denatured at 1M solution then
887 renatured through neutralization with HCl 24 hrs prior to readings. DMSO denaturation
888 conditions involved DMSO in water at 0%, 5% and 10%. For the DMSO renaturation
889 experiments, DMSO was removed by dialysis (see above) prior to spectrophotometer
890 readings. Absorbance readings were taken at 400-700 nm with 1 nm steps. We note
891 that DMSO alone induces a positive shift in the absorbance maximum of Congo Red.
892 This phenomenon mitigates against observation of the full extent of blue shift in Congo
893 Red between untreated glucan and DMSO denatured glucan and tends to reduce the
894 statistical significance of this comparison. Therefore, we present control values for
895 Congo Red with and without DMSO in our data presentation so that the extent of the
896 solvent's effect on the assay may be apparent. All experiments were conducted in
897 technical triplication across three independent experimental replicates.

898 **Fluorescence Lifetime Imaging Microscopy**

899 HEK-293 cells were plated at 25,000 cells in a 35 mm (MatTEK dishes) 48h prior to
900 imaging. Cells were transfected with Emerald-Dectin1A-N-10 and mCherry-Dectin1A-N-
901 10 24 hrs prior to imaging. FLIM-FRET images were obtained using a Leica DMi8
902 inverted microscope. A Leica Harmonic Compound PL apochromatic CS2 63X water
903 objective with a correction collar (1.2 NA) was used for imaging. A tunable & pulsed
904 White Light Laser (470 - 670 nm) was operated at 80 MHz at 3% laser power using a
905 488 nm notch filter to excite our sample. A scan speed of 200 and a 256 x 256
906 resolution was used. Two hybrid detectors collected at photons at (512-540 nm) and
907 (650-700 nm) respectively on the counting mode setting. Temperature was kept at 37
908 °C using a Tokai Hit Stage Top Incubator for Live Cell Imaging. Lifetime images were
909 collected using a Pico Harp 300 Fluorescence Lifetime Microscopy Time-Correlated
910 Single Photon Counting (TCSPC) system. For our glucan stimulated cells, prior to
911 stimulation 23 frames were collected. 230 frames were taken immediately after
912 stimulated with β-glucans at a concentration of 10 ug/ml. Analysis was conducted on
913 minute time points (1-5 minutes). For yeast contact site imaging studies, 3.5 x10^6 fixed
914 yeast cells were resuspended in 1 ml of PBS. 100 µl of the solution was added to HEK-
915 293 cells in 35 mm dishes 15 minutes prior to imaging. 23 frames were collected per
916 cell. Images were collected at a maximum of 45 minutes after the addition of yeast per
917 plate.

918 Analysis was conducted on the plasma membrane by masking out internal cellular
919 compartments on the images. For our fungal contact site studies, analysis was
920 conducted on the plasma membrane that was in contact with the fungus and a separate
921 masking for plasma membrane that was not in contact with any yeast. A bi-exponential

922 fit was performed to the decay curve. For donor only and donor-acceptor on opposite
923 sides of the plasma membrane (negative control) the decay curve indicated a negative
924 amplitude for one of the components, thus indicating a mono-exponential decay was a
925 more accurate representation. Therefore, decay curves from these samples were
926 analyzed using a mono-exponential fit. For cells with donor-acceptor on the cytosolic
927 tail, data was fit to a bi-exponential decay with the first lifetime component being locked
928 at the donor only lifetime of 2.4 ns (τ_D). Lifetime values of the second component (τ_{DA}) of
929 the decay curve were used to calculate FRET efficiency using the equation:
930 $FRET\ Efficiency = \left(1 - \frac{\tau DA}{\tau D}\right) \times 100$. To determine the number of receptors undergoing a
931 FRET process (Donor-acceptor Population), amplitude ratio between the first
932 component (AmpD) and the second component(AmpDA) was calculated according to
933 the following formula: $Donor - Acceptor\ Population = \frac{Amp\ DA}{(AmpD + AmpDA)} \times 100$.

934 **Raster Image Correlation Analysis/Number and Brightness**

935 Protocols on RICS and N&B analysis have been previously described in more depth
936 [55,77]. HEK-293 cells expressing Emerald-Dectin1A-C-10 were plated at 40,000 cells
937 in a 35 mm (MatTEK dishes) 24h prior to imaging. Images were collected at 256 x 256
938 resolution on a 60× 1.4 NA oil immersion objective lens (Olympus PlanApo/IR) with an
939 optical zoom of 16.4X (0.050 μm pixels). Data was collected using a GaAsP PMT
940 detector operated in photon counting mode. The 473 nm diode laser operated at 0.1%
941 laser power was used in these images. The Point Spread Function (PSF) radial beam
942 waist was estimated using 192 nM EFGP in solution and setting the diffusion coefficient
943 to 90 $\mu m^2/s$. Under these conditions the beam waist was determined to be 0.21 μm.

944 Immobile features were removed using a 4-frame moving average subtraction. Cells
945 were stimulated with a final concentration of 1 μg/ml of glucan. After stimulation, 200
946 frames were collected at a pixel dwell time of 4 μs/pixel (line scan of 1.096 ms) with a
947 pinhole size of 100 μm.

948 Images collected were also used for our Numbers and Brightness analysis, we used
949 192 nM EGFP in solution and purified mEmerald-GFP protein to set the average
950 brightness of our monomeric protein (Supplemental Fig. 3). Furthermore, the S-factor
951 was calculated using the background image. We divided each brightness distribution by
952 monomeric, dimeric, and oligomeric sections according to previous research [78]. The
953 cursors were scaled quadratically and centered at B values of 1.3, 1.6, and 2.35 for
954 monomers, dimers, and oligomers respectively.

955 **DSTORM analysis**

956 HEK-293 cells, were grown on cleaned and Poly-L-Lysine (0.1 mg/ml) coated coverslips
957 (~$5*10^4$ cells/coverslip) within wells of a six-well plate at 37°C 24hrs prior to the
958 experiment. The cells were then treated with MMW glucan at 1ug/ml for 50 second. The
959 cells were then fixed with paraformaldehyde (PFA; 4%) for 5 minutes at 37 °C followed
960 by three washes of PBS.

961 Data acquisition was on an Olympus IX-71 microscope equipped with an objective
962 based TIRF illuminator using an oil-immersion objective (PlanApo N, 150×/1.45 NA;
963 Olympus) in an oblique illumination configuration. Sample excitation was done using a
964 637nm laser (Thorlabs, laser diode HL63133DG), with custom-built collimation optics.

To minimize the drift that occurred during data acquisition, a self-registration algorithm was implemented.

The Dectin-1A nanodomain density was quantified by Super resolution imaging and analyzed using (HSET) as a clustering algorithm in MATLAB. The data for 34 cells for each condition were run through the first pass of HSET to collapse the observations of the blinking fluorophores into single estimates of the true locations of fluorophore [13]. The second HSET pass determined clustering using DBSCAN algorithm [79] which is depend on two parameters (minPts) that is the minimum number of object containing a multi-cluster and the maximum distance between the objects (epsilon). We optimized these parameters for the datasets used in this study at 3 and 27 nm respectively [65].

Collisional FRET Simulation with Monomeric Dectin-1

For this simulation, first a number of particles were generated based on the numbers of fluorophore molecules on the membrane in a specific volume on the real cell. As the experiments have shown that the ratio of donors to acceptors is roughly 50%, in our model 50% of particles were donors while the rest were of acceptors. The absolute number of donor and acceptor molecules was based on experimentally determined Dectin-1A membrane density presented in Fig. 4.

The initial location of each particle was defined by drawing random numbers from a uniform distribution. Throughout the simulation, particle movement was modeled by using a random walk process. The distance each particle moved at each time point was determined by the diffusion coefficient that was experimentally determined and reported in Fig. 4. All particle movements are independent of their type and status.

The simulation space included monomer molecules as donors and acceptors. This simulation space-corresponded to total area of 0.64 μm^2 (equivalent to ~20 pixels membrane area in an experimental FLIM dataset). The total duration of the simulation was 97.6 μs (equivalent to the total experimental data acquisition time for 20 pixels).

Each simulation run included 3904 sequential pulses with each pulse having the equal length of 25 ns (0.1 ns time resolution). At the start of each pulse, 30% donors were selected to act as excited particles. A lifetime value was assigned to each excited particle by generating a random number from an exponential probability density function (τ=2.4 ns; an experimentally determined value of our donor fluorophore). This lifetime value determined how long each excited donor remained excited.

At each time point, after the new location of all particles are calculated (using random walk process), each excited donor neighborhood is checked for acceptors. The neighborhood is defined as a disk with radius of 4-10 nm. In the case where there is an acceptor present in the neighborhood of a specific excited donor, the energy of donor is transferred to the acceptor (see “FRET efficiency” below), which essentially would mean that the donor has decayed. Please note that there are two different phenomena that would result in the decay of excited donors: FRET (as explained in this paragraph) and emission (where the excited donor decay to ground state, according to its characteristic fluorescence lifetime). The total probability of excited state decay is the sum of probabilities from both processes.

Simulation FRET efficiency

With the assumption that the concentration of excited donors is lower than acceptors, concentration, we can consider only one donor molecule. In addition, we assume that orientation factor for dipolar coupling between donor and acceptor is identical for all donor-acceptor pairs because donors and acceptors are considered to be rotating freely. Therefore the FRET efficiency equation is as follows: [80]

$$E = \frac{1}{1 + \sum_{i}^{N} (\frac{R_i}{R_0})^6}$$

The Förster distance (R_0) of the pair of donor and acceptor fluorophores simulated also matches that used for donors and acceptors in FLIM FRET experiments, namely R_0= 5.24 nm [81].The FRET efficiency in this simulation calculates the combination of FRET resulted by acceptors surrounding one excited donor, which are located at some distance from the donor within a specified maximum radial distance, as explained in *Results*.

Software

For the RICS and N&B Data presentation and analysis we used the SimFCS Program (www.lfd.uci.edu). The calcium imaging was analyzed using ImageJ. The FLIM-FRET results were analyzed using Symphotime64 software. The BioLayer interferometry analysis was done using BLItz Pro software. Statistical analysis was performed with GraphPad Prism versions 8.2 (GraphPad Software Inc.). DSTORM analysis and FLIM-FRET modeling was performed using MATLAB using our own algorithm (https://github.com/NeumannLab/FRET-Simulation).

Conflicts of Interest Statement

1029 EUA, AEA and AKN declare that they have no conflicts of interest relevant to this work.
1030 We acknowledge that MD and KM are employees of ImmunoResearch, Inc, which
1031 provided soluble glucans for this study. MD and KM conducted physicochemical
1032 analysis of these glucans and analyzed the results as reported above, but did not
1033 determine any other experimental design or data interpretation decisions involved in the
1034 work.

1035 **Acknowledgements**

1036 This research was supported by the University of New Mexico Center for
1037 Spatiotemporal Modeling of Cell Signaling (STMC; NIH P50GM085273, AKN) and
1038 R01AI116894 (AKN), EUA was supported by fellowships from the STMC and an NIH
1039 T32 training grant (NIH T32 AI007538) during the course of this work. We acknowledge
1040 the competent technical assistance of Ms. Zinia Pervin in relation to BLI determinations
1041 of Dectin-1A/glucan affinity. We acknowledge Diane Lidke for the many helpful
1042 discussions on FLIM-FRET and her critical reading and discussion of the manuscript.

1043

1044 **References**

1045 1. Cleveland AA, Harrison LH, Farley MM, Hollick R, Stein B, Chiller TM, et al.
1046 Declining Incidence of Candidemia and the Shifting Epidemiology of Candida
1047 Resistance in Two US Metropolitan Areas, 2008–2013: Results from Population-
1048 Based Surveillance. Chowdhary A, editor. PLoS One. 2015;10: e0120452.
1049 doi:10.1371/journal.pone.0120452

1050 2. Pfaller MA, Diekema DJ. Epidemiology of invasive candidiasis: a persistent public

1051 health problem. Clin Microbiol Rev. 2007;20: 133–63. doi:10.1128/CMR.00029-06

1052 3. Cleveland AA, Farley MM, Harrison LH, Stein B, Hollick R, Lockhart SR, et al.
1053 Changes in incidence and antifungal drug resistance in candidemia: results from
1054 population-based laboratory surveillance in Atlanta and Baltimore, 2008-2011.
1055 Clin Infect Dis. 2012;55: 1352–61. doi:10.1093/cid/cis697

1056 4. Kao AS, Brandt ME, Pruitt WR, Conn LA, Perkins BA, Stephens DS, et al. The
1057 Epidemiology of Candidemia in Two United States Cities: Results of a Population-
1058 Based Active Surveillance. Clin Infect Dis. 1999;29: 1164–1170.
1059 doi:10.1086/313450

1060 5. Hajjeh RA, Sofair AN, Harrison LH, Lyon GM, Arthington-Skaggs BA, Mirza SA, et
1061 al. Incidence of bloodstream infections due to Candida species and in vitro
1062 susceptibilities of isolates collected from 1998 to 2000 in a population-based
1063 active surveillance program. J Clin Microbiol. 2004;42: 1519–27.
1064 doi:10.1128/JCM.42.4.1519-1527.2004

1065 6. Antibiotic Resistance Threats in the United States, 2013 | Antibiotic/Antimicrobial
1066 Resistance | CDC [Internet]. [cited 24 Jul 2018]. Available:
1067 https://www.cdc.gov/drugresistance/threat-report-2013/index.html

1068 7. Chaffin WL. Candida albicans Cell Wall Proteins. Microbiol Mol Biol Rev. 2008;72:
1069 495–544. doi:10.1128/mmbr.00032-07

1070 8. Ruiz-Herrera J, Victoria Elorza M, ValentÃ-n E, Sentandreu R. Molecular
1071 organization of the cell wall of *Candida albicans* and its relation to pathogenicity.
1072 FEMS Yeast Res. 2006;6: 14–29. doi:10.1111/j.1567-1364.2005.00017.x

1073 9. Gow NAR, Hube B. Importance of the Candida albicans cell wall during
1074 commensalism and infection. Current Opinion in Microbiology. 2012. pp. 406–
1075 412. doi:10.1016/j.mib.2012.04.005

1076 10. Ballou ER, Avelar GM, Childers DS, Mackie J, Bain JM, Wagener J, et al. Lactate
1077 signalling regulates fungal β-glucan masking and immune evasion. Nat Microbiol.
1078 2016;2. doi:10.1038/nmicrobiol.2016.238

1079 11. Sherrington SL, Sorsby E, Mahtey N, Kumwenda P, Lenardon MD, Brown I, et al.
1080 Adaptation of Candida albicans to environmental pH induces cell wall remodelling
1081 and enhances innate immune recognition. PLoS Pathog. 2017;13.
1082 doi:10.1371/journal.ppat.1006403

1083 12. Hopke A, Nicke N, Hidu EE, Degani G, Popolo L, Wheeler RT. Neutrophil Attack
1084 Triggers Extracellular Trap-Dependent Candida Cell Wall Remodeling and Altered
1085 Immune Recognition. PLoS Pathog. 2016;12. doi:10.1371/journal.ppat.1005644

1086 13. Lin J, Wester MJ, Graus MS, Lidke KA, Neumann AK. Nanoscopic cell-wall
1087 architecture of an immunogenic ligand in Candida albicans during antifungal drug
1088 treatment. Mol Biol Cell. 2016;27: 1002–14. doi:10.1091/mbc.E15-06-0355

1089 14. Pappas HC, Sylejmani R, Graus MS, Donabedian PL, Whitten DG, Neumann AK.
1090 Antifungal Properties of Cationic Phenylene Ethynylenes and Their Impact on β-
1091 Glucan Exposure. Antimicrob Agents Chemother. 2016;60: 4519–29.
1092 doi:10.1128/AAC.00317-16

1093 15. Wheeler RT, Kombe D, Agarwala SD, Fink GR. Dynamic, morphotype-specific
1094 Candida albicans β-glucan exposure during infection and drug treatment. PLoS

1095 Pathog. 2008;4. doi:10.1371/journal.ppat.1000227

1096 16. Wheeler RT, Fink GR. A drug-sensitive genetic network masks fungi from the
1097 immune system. PLoS Pathog. 2006;2: 328–339.
1098 doi:10.1371/journal.ppat.0020035

1099 17. Sletmoen M, Stokke BT. Higher order structure of (1,3)-β-D-glucans and its
1100 influence on their biological activities and complexation abilities. Biopolymers.
1101 2008;89: 310–321. doi:10.1002/bip.20920

1102 18. Young SH, Dong WJ, Jacobs RR. Observation of a partially opened triple-helix
1103 conformation in 1→3-β- glucan by fluorescence resonance energy transfer
1104 spectroscopy. J Biol Chem. 2000;275: 11874–11879.
1105 doi:10.1074/jbc.275.16.11874

1106 19. Chuah CT, Sarko A, Deslandes Y, Marchessault RH. Triple-Helical Crystalline
1107 Structure of Curdlan and Paramylon Hydrates1 [Internet]. Macromolecules. 1983.
1108 Available: https://pubs.acs.org/sharingguidelines

1109 20. Yoshioka Y, Uehara N, Saitô H. Conformation-dependent change in antitumor
1110 activity of linear and branched (1----3)-beta-D-glucans on the basis of
1111 conformational elucidation by carbon-13 nuclear magnetic resonance
1112 spectroscopy. Chem Pharm Bull (Tokyo). 1992;40: 1221–6.
1113 doi:10.1248/cpb.40.1221

1114 21. Okobira T, Miyoshi K, Uezu K, Sakurai K, Shinkai S. Molecular dynamics studies
1115 of side chain effect on the β-1,3-D-glucan triple helix in aqueous solution.
1116 Biomacromolecules. 2008;9: 783–788. doi:10.1021/bm700511d

1117 22. Chihara G, Hamuro J, Maeda Y, Arai Y, Fukuoka F. Fractionation and purification
1118 of the polysaccharides with marked antitumor activity, especially lentinan, from
1119 Lentinus edodes (Berk.) Sing. (an edible mushroom). Cancer Res. 1970;30:
1120 2776–81. Available: http://www.ncbi.nlm.nih.gov/pubmed/5530561

1121 23. Zhou L, Zhang Q, Zhang Y, Liu J, Cao Y. The shiitake mushroom-derived
1122 immuno-stimulant lentinan protects against murine malaria blood-stage infection
1123 by evoking adaptive immune-responses. Int Immunopharmacol. 2009;9: 455–62.
1124 doi:10.1016/j.intimp.2009.01.010

1125 24. Brown GD, Gordon S. Fungal β-Glucans and Mammalian Immunity. Immunity.
1126 2003;19: 311–315. doi:10.1016/S1074-7613(03)00233-4

1127 25. Novak M, Vetvicka V.) β-Glucans, History, and the Present: Immunomodulatory
1128 Aspects and Mechanisms of Action. J Immunotoxicol. 2008;5: 47–57.
1129 doi:10.1080/15476910802019045

1130 26. Kim HS, Hong JT, Kim Y, Han S-B. Stimulatory Effect of β-glucans on Immune
1131 Cells. Immune Netw. 2011;11: 191. doi:10.4110/in.2011.11.4.191

1132 27. Mueller A, Raptis J, Rice PJ, Kalbfleisch JH, Stout RD, Ensley HE, et al. The
1133 influence of glucan polymer structure and solution conformation on binding to (1--
1134 >3)-beta-D-glucan receptors in a human monocyte-like cell line. Glycobiology.
1135 2000;10: 339–46. Available: http://www.ncbi.nlm.nih.gov/pubmed/10764821

1136 28. Zhang L, Li X, Xu X, Zeng F. Correlation between antitumor activity, molecular
1137 weight, and conformation of lentinan. Carbohydr Res. 2005;340: 1515–21.
1138 doi:10.1016/j.carres.2005.02.032

1139 29. Elder MJ, Webster SJ, Chee R, Williams DL, Hill Gaston JS, Goodall JC. β-
1140 Glucan Size Controls Dectin-1-Mediated Immune Responses in Human Dendritic
1141 Cells by Regulating IL-1β Production. Front Immunol. 2017;8: 791.
1142 doi:10.3389/fimmu.2017.00791

1143 30. Di Luzio NR, Williams DL, McNamee RB, Edwards BF, Kitahama A. Comparative
1144 tumor-inhibitory and anti-bacterial activity of soluble and particulate glucan. Int J
1145 cancer. 1979;24: 773–9. doi:10.1002/ijc.2910240613

1146 31. Tzianabos AO. Polysaccharide immunomodulators as therapeutic agents:
1147 structural aspects and biologic function. Clin Microbiol Rev. 2000;13: 523–33.
1148 doi:10.1128/cmr.13.4.523-533.2000

1149 32. Wang Y, Zhang L, Li Y, Hou X, Zeng F. Correlation of structure to antitumor
1150 activities of five derivatives of a β-glucan from Poria cocos sclerotium. Carbohydr
1151 Res. 2004;339: 2567–2574. doi:10.1016/j.carres.2004.08.003

1152 33. Smith AJ, Graves B, Child R, Rice PJ, Ma Z, Lowman DW, et al.
1153 Immunoregulatory Activity of the Natural Product Laminarin Varies Widely as a
1154 Result of Its Physical Properties. J Immunol. 2018;200: 788–799.
1155 doi:10.4049/jimmunol.1701258

1156 34. Suzuki T, Ohno N, Saito K, Yadomae T. Activation of the complement system by
1157 (1----3)-beta-D-glucans having different degrees of branching and different
1158 ultrastructures. J Pharmacobiodyn. 1992;15: 277–85. Available:
1159 http://www.ncbi.nlm.nih.gov/pubmed/1432567

1160 35. Maeda YY, Watanabe ST, Chihara C, Rokutanda M. Denaturation and

1161 renaturation of a beta-1,6;1,3-glucan, lentinan, associated with expression of T-
1162 cell-mediated responses. Cancer Res. 1988;48: 671–5. Available:
1163 http://www.ncbi.nlm.nih.gov/pubmed/2446749

1164 36. Yanaki T, Ito W, Tabata K, Kojima T, Norisuye T, Takano N, et al. Correlation
1165 between the antitumor activity of a polysaccharide schizophyllan and its triple-
1166 helical conformation in dilute aqueous solution. Biophys Chem. 1983;17: 337–
1167 342. doi:10.1016/0301-4622(83)80018-0

1168 37. Mueller A, Raptis J, Rice PJ, Kalbfleisch JH, Stout RD, Ensley HE, et al. The
1169 influence of glucan polymer structure and solution conformation on binding to
1170 (1→3)-β-D-glucan receptors in a human monocyte-like cell line. Glycobiology.
1171 2000;10: 339–346. doi:10.1093/glycob/10.4.339

1172 38. Duggan S, Leonhardt I, Hünniger K, Kurzai O. Host response to *Candida albicans*
1173 bloodstream infection and sepsis. Virulence. 2015; 1–11.
1174 doi:10.4161/21505594.2014.988096

1175 39. Davis SE, Hopke A, Minkin SC, Montedonico AE, Wheeler RT, Reynolds TB, et
1176 al. Masking of β(1-3)-glucan in the cell wall of Candida albicans from detection by
1177 innate immune cells depends on phosphatidylserine. Infect Immun. 2014;82:
1178 4405–13. doi:10.1128/IAI.01612-14

1179 40. Gow NAR, Netea MG, Munro CA, Ferwerda G, Bates S, Mora-Montes HM, et al.
1180 Immune recognition of Candida albicans beta-glucan by dectin-1. J Infect Dis.
1181 2007;196: 1565–71. doi:10.1086/523110

1182 41. Brown GD, Taylor PR, Reid DM, Willment JA, Williams DL, Martinez-Pomares L,

1183 et al. Dectin-1 is a major β-glucan receptor on macrophages. J Exp Med.
1184 2002;196: 407–412. doi:10.1084/jem.20020470

1185 42. Rice PJ, Adams EL, Ozment-Skelton T, Gonzalez AJ, Goldman MP, Lockhart BE,
1186 et al. Oral delivery and gastrointestinal absorption of soluble glucans stimulate
1187 increased resistance to infectious challenge. J Pharmacol Exp Ther. 2005;314:
1188 1079–86. doi:10.1124/jpet.105.085415

1189 43. O'Neill SK, Getahun A, Gauld SB, Merrell KT, Tamir I, Smith MJ, et al.
1190 Monophosphorylation of CD79a and CD79b ITAM motifs initiates a SHIP-1
1191 phosphatase-mediated inhibitory signaling cascade required for B cell anergy.
1192 Immunity. 2011;35: 746–756. doi:10.1016/j.immuni.2011.10.011

1193 44. Tomohiro Kurosaki B, AJohnson S, Pao L, Sada K, HirohelYamamura Il, Cambier
1194 JC. Role of the Syk Autophosphorylation Site and SH2 Domains in B Cell Antigen
1195 Receptor Signaling. doi:10.1084/jem.182.6.1815

1196 45. Hughes CE, Pollitt AY, Mori J, Eble JA, Tomlinson MG, Hartwig JH, et al. CLEC-2
1197 activates Syk through dimerization. Blood. 2010;115: 2947–55.
1198 doi:10.1182/blood-2009-08-237834

1199 46. Bartel Y, Bauer B, Steinle A. Modulation of NK cell function by genetically coupled
1200 C-type lectin-like receptor/ligand pairs encoded in the human natural killer gene
1201 complex. Front Immunol. 2013;4: 362. doi:10.3389/fimmu.2013.00362

1202 47. Hino S, Kito A, Yokoshima R, Sugino R, Oshima K, Morita T, et al. Discharge of
1203 solubilized and Dectin-1-reactive β-glucan from macrophage cells phagocytizing
1204 insoluble β-glucan particles: Involvement of reactive oxygen species (ROS)-driven

1205 degradation. Biochem Biophys Res Commun. 2012;421: 329–334.
1206 doi:10.1016/j.bbrc.2012.04.009

1207 48. Hong F, Yan J, Baran JT, Allendorf DJ, Hansen RD, Ostroff GR, et al. Mechanism
1208 by which orally administered beta-1,3-glucans enhance the tumoricidal activity of
1209 antitumor monoclonal antibodies in murine tumor models. J Immunol. 2004;173:
1210 797–806. doi:10.4049/jimmunol.173.2.797

1211 49. Gonzalez JA, Digby JD, Rice PJ, Breuel KF, DePonti WK, Kalbfleisch JH, et al. At
1212 low serum glucan concentrations there is an inverse correlation between serum
1213 glucan and serum cytokine levels in ICU patients with infections. Int
1214 Immunopharmacol. 2004;4: 1107–1115. doi:10.1016/J.INTIMP.2004.05.010

1215 50. Digby J, Kalbfleisch J, Glenn A, Larsen A, Browder W, Williams D. Serum glucan
1216 levels are not specific for presence of fungal infections in intensive care unit
1217 patients. Clin Diagn Lab Immunol. 2003;10: 882–5. doi:10.1128/cdli.10.5.882-
1218 885.2003

1219 51. Lowman DW, Ferguson DA, Williams DL. Structural characterization of (1 0/ 3)-b-
1220 D-glucans isolated from blastospore and hyphal forms of Candida albicans.
1221 doi:10.1016/S0008-6215(03)00169-1

1222 52. Kogan G, Alföldi J, Masler L. 13C-nmr spectroscopic investigation of two yeast
1223 cell wall β-D-glucans. Biopolymers. 1988;27: 1055–1063.
1224 doi:10.1002/bip.360270702

1225 53. Nitschke J, Modick H, Busch E, von Rekowski RW, Altenbach H-J, Mölleken H. A
1226 new colorimetric method to quantify β-1,3-1,6-glucans in comparison with total β-

1227 1,3-glucans in edible mushrooms. Food Chem. 2011;127: 791–796.
1228 doi:10.1016/J.FOODCHEM.2010.12.149

1229 54. Brown CM, Dalal RB, Hebert B, Digman MA, Horwitz AR, Gratton E. Raster
1230 image correlation spectroscopy (RICS) for measuring fast protein dynamics and
1231 concentrations with a commercial laser scanning confocal microscope. J Microsc.
1232 2008;229: 78–91. doi:10.1111/j.1365-2818.2007.01871.x

1233 55. Digman MA, Stakic M, Gratton E. Raster image correlation spectroscopy and
1234 number and brightness analysis. Methods Enzymol. 2013;518: 121–44.
1235 doi:10.1016/B978-0-12-388422-0.00006-6

1236 56. Bauer B, Steinle A. HemITAM: A single tyrosine motif that packs a punch. Sci
1237 Signal. 2017;10: 1–10. doi:10.1126/scisignal.aan3676

1238 57. Brown GD. Dectin-1: a signalling non-TLR pattern-recognition receptor. Nat Rev
1239 Immunol. 2006;6: 33–43. doi:10.1038/nri1745

1240 58. Brown J, O'Callaghan CA, Marshall ASJ, Gilbert RJC, Siebold C, Gordon S, et al.
1241 Structure of the fungal beta-glucan-binding immune receptor dectin-1: implications
1242 for function. Protein Sci. 2007;16: 1042–52. doi:10.1110/ps.072791207

1243 59. Dulal HP, Adachi Y, Ohno N, Yamaguchi Y. β-Glucan-induced cooperative
1244 oligomerization of Dectin-1 C-type lectin-like domain. Glycobiology. 2018;28: 612–
1245 623. doi:10.1093/glycob/cwy039

1246 60. Singh DR, Kanvinde P, King C, Pasquale EB, Hristova K. The EphA2 receptor is
1247 activated through induction of distinct, ligand-dependent oligomeric structures.

1248 Commun Biol. 2018;1: 15. doi:10.1038/s42003-018-0017-7

1249 61. Digman MA, Dalal R, Horwitz AF, Gratton E. Mapping the number of molecules
1250 and brightness in the laser scanning microscope. Biophys J. 2008;94: 2320–32.
1251 doi:10.1529/biophysj.107.114645

1252 62. Unruh JR, Gratton E. Analysis of molecular concentration and brightness from
1253 fluorescence fluctuation data with an electron multiplied CCD camera. Biophys J.
1254 2008;95: 5385–98. doi:10.1529/biophysj.108.130310

1255 63. Trullo A, Corti V, Arza E, Caiolfa VR, Zamai M. Application limits and data
1256 correction in number of molecules and brightness analysis. Microsc Res Tech.
1257 2013;76: 1135–1146. doi:10.1002/jemt.22277

1258 64. Wester MJ, Lin J, Neumann AK. A computational model for regulation of
1259 nanoscale glucan exposure in Candida albicans. PLoS One. 2017;12.
1260 doi:10.1371/journal.pone.0188599

1261 65. Graus MS, Wester MJ, Lowman DW, Williams DL, Kruppa MD, Martinez CM, et
1262 al. Mannan Molecular Substructures Control Nanoscale Glucan Exposure in
1263 Candida. Cell Rep. 2018;24: 2432-2442.e5. doi:10.1016/j.celrep.2018.07.088

1264 66. OKAZAKI M, ADACHI Y, OHNO N, YADOMAE T. Structure-Activity Relationship
1265 of (1.RAR.3)-.BETA.-D-Glucans in the Induction of Cytokine Production from
1266 Macrophages, in Vitro. Biol Pharm Bull. 1995;18: 1320–1327.
1267 doi:10.1248/bpb.18.1320

1268 67. Cleary JA, Kelly GE, Husband AJ. The effect of molecular weight and β-1,6-

1269 linkages on priming of macrophage function in mice by (1,3)-β- d -glucan.
1270 Immunol Cell Biol. 1999;77: 395–403. doi:10.1046/j.1440-1711.1999.00848.x

1271 68. Itano MS, Graus MS, Pehlke C, Wester MJ, Liu P, Lidke KA, et al. Super-
1272 resolution imaging of C-type lectin spatial rearrangement within the dendritic cell
1273 plasma membrane at fungal microbe contact sites. Front Phys. 2014;2.
1274 doi:10.3389/fphy.2014.00046

1275 69. Feinberg H, Guo Y, Mitchell DA, Drickamer K, Weis WI. Extended neck regions
1276 stabilize tetramers of the receptors DC-SIGN and DC-SIGNR. J Biol Chem.
1277 2005;280: 1327–35. doi:10.1074/jbc.M409925200

1278 70. Vitale M, Falco M, Castriconi R, Parolini S, Zambello R, Semenzato G, et al.
1279 Identification of NKp80, a novel triggering molecule expressed by human NK
1280 cells. Eur J Immunol. 2001;31: 233–242. doi:10.1002/1521-
1281 4141(200101)31:1<233::AID-IMMU233>3.0.CO;2-4

1282 71. Hanč P, Schulz O, Fischbach H, Martin SR, Kjær S, Reis e Sousa C. A pH- and
1283 ionic strength-dependent conformational change in the neck region regulates
1284 DNGR-1 function in dendritic cells. EMBO J. 2016;35: 2484–2497.
1285 doi:10.15252/embj.201694695

1286 72. Ariizumi K, Shen GL, Shikano S, Xu S, Ritter R, Kumamoto T, et al. Identification
1287 of a novel, dendritic cell-associated molecule, dectin-1, by subtractive cDNA
1288 cloning. J Biol Chem. 2000;275: 20157–67. doi:10.1074/jbc.M909512199

1289 73. Goodridge HS, Reyes CN, Becker CA, Katsumoto TR, Ma J, Wolf AJ, et al.
1290 Activation of the innate immune receptor Dectin-1 upon formation of a “phagocytic

1291 synapse". Nature. 2011;472: 471–5. doi:10.1038/nature10071

1292 74. Graus MS, Pehlke C, Wester MJ, Davidson LB, Steinberg SL, Neumann AK. A
1293 New Tool to Quantify Receptor Recruitment to Cell Contact Sites during Host-
1294 Pathogen Interaction. Gabhann F Mac, editor. PLoS Comput Biol. 2014;10:
1295 e1003639. doi:10.1371/journal.pcbi.1003639

1296 75. Needs PW, Selvendran RR. Avoiding oxidative degradation during sodium
1297 hydroxide/methyl iodide-mediated carbohydrate methylation in dimethyl sulfoxide.
1298 Carbohydr Res. 1993;245: 1–10. doi:10.1016/0008-6215(93)80055-J

1299 76. Kim YT, Kim EH, Cheong C, Williams DL, Kim CW, Lim ST. Structural
1300 characterization of β-D-(1 → 3, 1 → 6)-linked glucans using NMR spectroscopy.
1301 Carbohydr Res. 2000;328: 331–341. doi:10.1016/S0008-6215(00)00105-1

1302 77. Youker RT, Teng H. Measuring protein dynamics in live cells: protocols and
1303 practical considerations for fluorescence fluctuation microscopy. J Biomed Opt.
1304 2014;19: 090801. doi:10.1117/1.jbo.19.9.090801

1305 78. Planes N, Digman MA, Vanderheyden PPML, Gratton E, Caballero-George C.
1306 Number and brightness analysis to study spatio-temporal distribution of the
1307 angiotensin II AT1 and the endothelin-1 ETA receptors: Influence of ligand
1308 binding. Biochim Biophys Acta - Gen Subj. 2019;1863: 917–924.
1309 doi:10.1016/J.BBAGEN.2019.03.004

1310 79. Ester M, Ester M, Kriegel H-P, Sander J, Xu X. A density-based algorithm for
1311 discovering clusters in large spatial databases with noise. 1996; 226--231.
1312 Available: http://citeseer.ist.psu.edu/viewdoc/summary?doi=10.1.1.121.9220

80. Wolber PK, Hudson BS. An analytic solution to the Förster energy transfer problem in two dimensions. Biophys J. 1979;28: 197–210. doi:10.1016/S0006-3495(79)85171-1

81. Akrap N, Seidel T, Barisas BG. Förster distances for fluorescence resonant energy transfer between mCherry and other visible fluorescent proteins. Anal Biochem. 2010;402: 105–106. doi:10.1016/J.AB.2010.03.026

Supplemental Materials

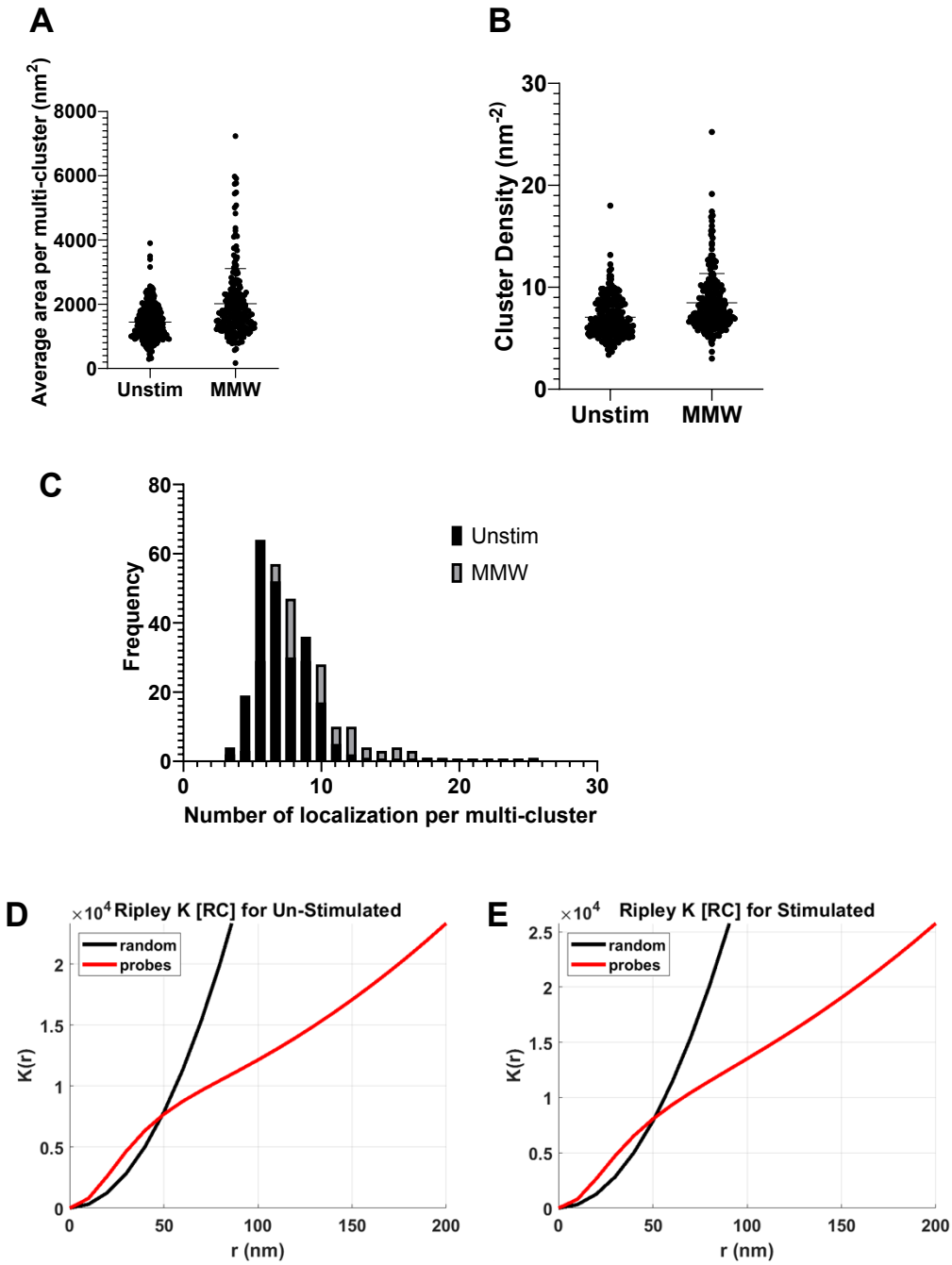

Supplemental Figure 1: DSTORM Clustering Analysis

(A) Average area of multi-cluster in dSTORM analysis of HEK-293 cells expressing Dectin-1A unstimulated or stimulated with MMW. (B) Cluster density of DSTORM analysis of HEK-293 cells expressing Dectin-1A unstimulated or stimulated with MMW. (C) Histogram analysis of the number of

1331 localizations of HEK-293 cells expressing Dectin-1A unstimulated or stimulated with MMW. (D) Spatial
1332 point pattern analysis with Ripley's K function of HEK-293 cells expressing Dectin-1A unstimulated or
1333 stimulated with (E) MMW. Data shown as mean ± SD (n = 34)

1334

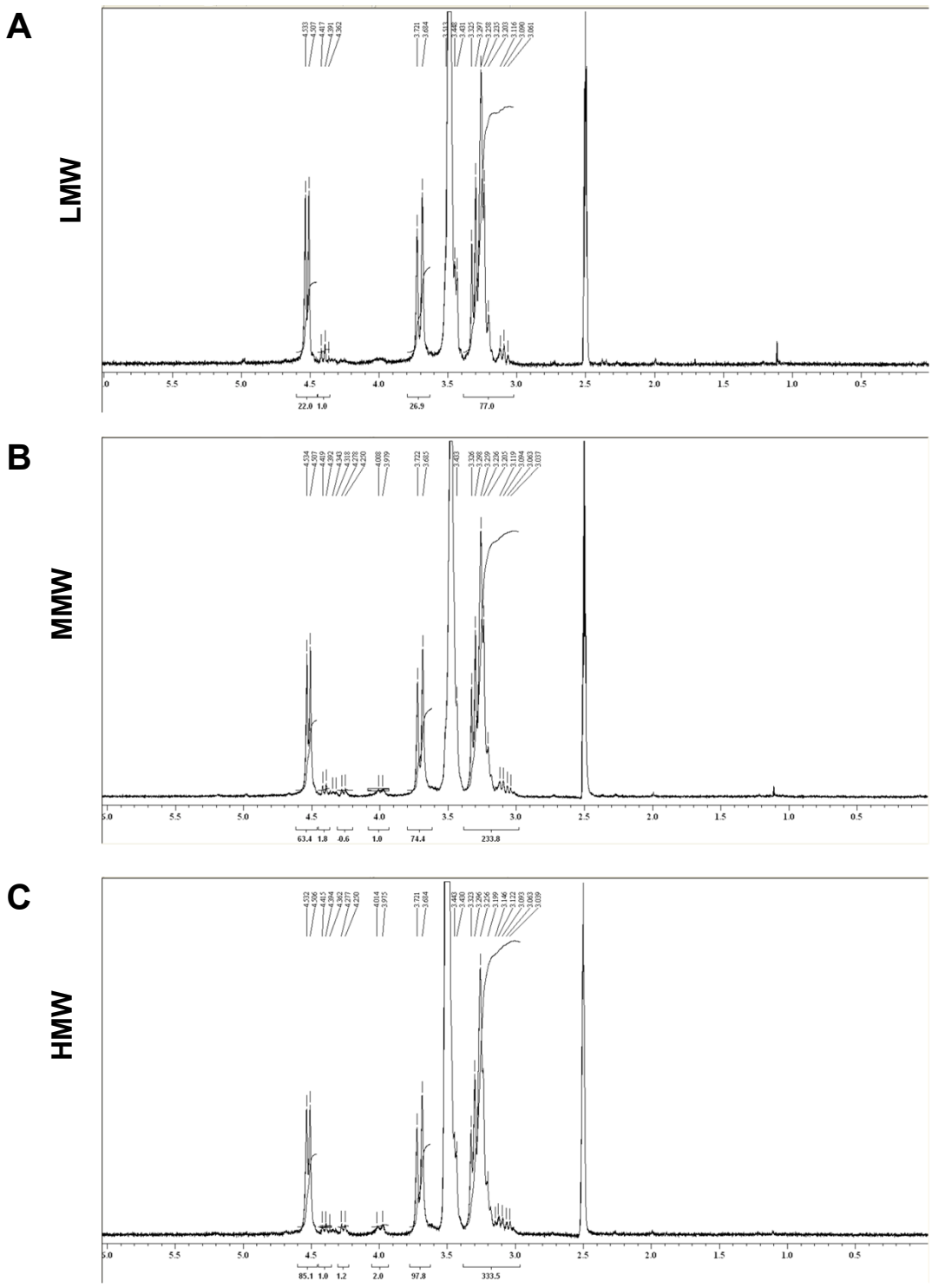

1335

1336 **Supplemental Figure 2: ^{1}HNMR Spectrum**

1337 (A) ^{1}HNMR spectrum of LMW, (B) MMW, and (C) HMW.

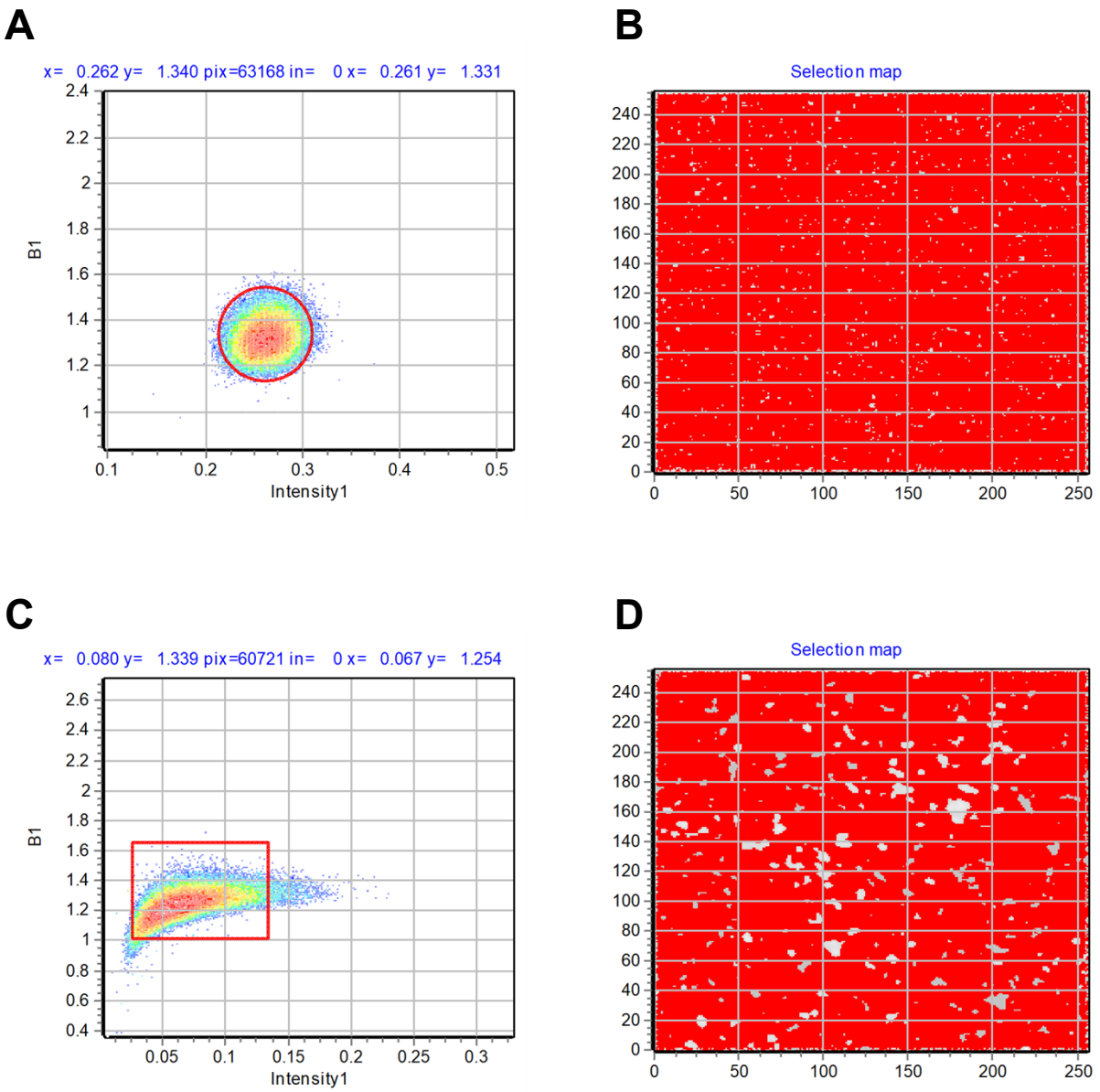

1338

1339 **Supplemental Figure 3: Numbers and brightness analysis calibration**

1340 (A) Brightness vs intensity 2D histogram of purified EGFP or mEmerald-Dectin-1A (C) with the selected
1341 pixels that contribute to the monomers (red) in the image. (B) Representative selection map of purified
1342 EGFP or mEmerald-Dectin-1A (D) in which the fluorescent protein populations are defined by colored
1343 cursors selected in the Brightness vs intensity histogram.

1344

1345

1346 **Supplemental Table 1.**

Table of Values

	LMW	MMW	HMW
Max Calcium Amplitude	1.2	2.5	1.8

	LMW	MMW	HMW	MMW Denatured	MMW Renatured
Kd (nM)	1.93	1.62	0.43	1.02	1.22

	LMW		MMW		HMW		MMW Denatured	
Min	FRET Efficiency %	Donor-Acceptor %	FRET Efficiency %	Donor-Acceptor %	FRET Efficiency %	Donor-Acceptor %	FRET Efficiency %	Donor-Acceptor %
0	83.3	17.7	76.5	15.3	86.1	14.5	87.5	15.9
1	79.1	17.1	77.0	22.8	80.1	19.5	86.7	15.8
2	79.1	17.9	74.3	22.1	78.9	19.8	86.2	15.1
3	78.5	18.1	77.1	23.7	78.9	21.7	86.3	15.2
4	78.2	19.5	72.1	25.7	79.5	22.5	84.1	16.1
5	77.9	18.8	71.9	28.2	79.5	23.7	84.5	14.1

	N&B			RICS	
	Monomers %	Dimers %	Oligomers %	Diffusion Coefficient ($\mu m^2/s$)	Number of Receptors/μm^2
Unstimulated	74.0	21.4	4.6	1.12	4608
LMW	69.5	20.6	9.9	0.90	3920
MMW	27.5	52.5	20.0	0.37	1768
HMW	37.5	48.7	13.8	0.37	1942

	Singlet Cluster Density (nm^{-2})	Multiple Cluster Density (nm^{-2})	Density of Localizations (nm^{-2})	Average Area per cluster(nm^2)
Unstimulated	0.74	0.59	7.06	1444
MMW	0.77	0.66	8.47	2016

	FRET Efficiency %	Donor- Acceptor %
Cell Membrane	81.8	15.7
SC5314	84.8	15.9
TRL035	78.8	25.1
Glucan Particle	78.8	29.6

1347